LJMU Research Online

Liu, Y, Liu, J, Zhang, Q, Liu, Y and Wang, Y

 Effect of dynamic safety distance of heterogeneous traffic flows on ship traffic efficiency: A prediction and simulation approach

http://researchonline.ljmu.ac.uk/id/eprint/23327/

Article

For more information please contact researchonline@ljmu.ac.uk

Research paper

Effect of dynamic safety distance of heterogeneous traffic flows on ship traffic efficiency: A prediction and simulation approach

Yang Liu [a,b], Jingxian Liu [a,b,c], Qian Zhang [d,*], Yi Liu [a,b,c,**], Yukuan Wang [a,b]

[a] School of Navigation, Wuhan University of Technology, 430063, China
[b] State Key Laboratory of Maritime Technology and Safety, Wuhan University of Technology, Wuhan, 430063, China
[c] National Engineering Research Center for Water Transport Safety, Wuhan University of Technology, 430063, China
[d] School of Engineering, Liverpool John Moores University, Liverpool, L3 3AF, UK

ARTICLE INFO

ABSTRACT

Compared to the heterogeneous traffic flow on roads, the heterogeneous characteristics of maritime traffic flow are more pronounced, due to disparities in the manoeuvrability, size, and safety requirements among different ships. These factors increase the complexity of quantifying traffic efficiency. This paper employs hierarchical clustering to categorise trajectories with similar speed variation features and utilises Long Short-Term Memory (LSTM) models to predict ship speeds, forming a speed control strategy based on time-series data. Moreover, extending from the principles of car-following, models are developed to compute dynamic safety distances for both manned and autonomous ships. Further, a port waterway simulation model based on cellular automaton (CA) is developed, integrating data-driven speed control strategies while maintaining dynamic safety distances, resulting in a comprehensive simulation model with dual speed control mechanisms. A case study of the Tianjin port shows the advantages of dynamic safety distances. Dynamic safety distances significantly improved ship navigation and overall channel traffic efficiency. The inclusion of autonomous ships further improves the efficiency and the benefits are directly related to the proportion of autonomous ships. This research provides new insights and methodologies for assessing transport efficiency and waterway capacity, which also offers support for research on autonomous maritime traffic flow.

1. Introduction

With the development of global economic integration, maritime transportation business has witnessed further growth, culminating in China achieving the world's highest cargo throughput and container throughput in2022.[1] It can be foreseen that the maritime transport industry will sustain a continuous growth trend in the future. Consequently, the traffic flow of ships entering and leaving a port will become more complex, posing higher demands on maritime authorities in terms of traffic organization and regulatory coordination. As an essential component of the port navigation system and a primary object of regulation by the supervisory authorities, the pressure facing the channels for entering and leaving the port will further intensify. Channel transport efficiency, serving as a key indicator reflecting the service of ships entering and leaving the port, is related to the planning,

organization, and operation of the entire port navigation system. The scientific and accurate quantification of it holds significant theoretical and practical value and remains a current hotspot and challenge in research.

Autonomous ship is a new type of ship that only needs a few crew members on board or at remote control stations to realise autonomous functions and perform various operations (Schröder et al., 2019), and the development of autonomous ships basically follows the research and development path of "assisted, decision-making-remote, control-unmanned, to autonomy'. In recent years, autonomous ships related technologies, such as artificial intelligence (Veitch and Alsos, 2022), situational awareness (Lin et al., 2022), and autonomous collision avoidance, gradually promote autonomous ships from imagination to reality. The development and application of autonomous ships have brought new changes to the ship traffic flow, the heterogeneous traffic

pattern of mixing autonomous ships and manned ships will continue to exist, and the coupling between the main bodies will be more complex. The research on the efficiency of heterogeneous ship traffic flow will face a new challenge, and how to quantify the impact of autonomous ships on the structure and efficiency of the traffic flow will become a problem that needs to be solved urgently.

In this paper, based on the characteristics of ship traffic flow, such as ship speed distribution, ship distance and ship type distribution, a ship traffic flow simulation model is established. The model is grounded on the dual-speed control strategy involving speed prediction and dynamic safety distance. The specific contributions include.

a. By employing advanced techniques such as Dynamic Time Warping (DTW) and hierarchical clustering methods, we have systematically clustered ship trajectories. This clustering is based on observed variations in speed, forming distinct categories reflecting different navigational behaviours. Subsequently, a predictive model employing a Long Short-Term Memory (LSTM) network has been established. This model is adept at predicting ship speed variations based on positional data, thereby contributing to a nuanced understanding of ship movements and speed alterations within navigational routes.

b. Integrating foundational theoretical frameworks with meticulously derived formulae, we have formulated a model to calculate a ship's reversing surge. This integration results in a robust and versatile model capable of determining the dynamic safety distance of ships.

c. Incorporating insights from Points a and b, we have developed a scalable Cellular Automaton (CA) model, enriched with two integral modules to elevate the fidelity of our simulations. The first module, Ship Speed Control, utilises the findings from speed classification in Point a to craft accurate speed control strategies for various ship types navigating through waterways. Additionally, the second module, named Dynamic Ship Safety Distance, introduces algorithms informed by the theoretical advancements made in Point b. This module is crucial for simulating the relative safety distances between both manned and autonomous ships under dynamic conditions. Together, these enhancements harness the knowledge gained from the preceding sections, offering a refined approach to modelling dynamic safety distances in maritime navigation.

The remainder of the paper is organised as follows: Section 2 introduces the latest research developments in the related fields, Section 3 describes the methods and models used, Section 4 applies the model to the main channel of Tianjin Port for empirical validation, and Section 5 discusses the model and offers insights into future research directions.

2. Literature review

To study the characteristics and efficiency of heterogeneous traffic flows resulted from the introduction of autonomous ships, it's imperative to commence with foundational traffic models, undertaking systematic modelling and analysis. This research primarily zeroes in on the speed control strategies based on predictions within traffic simulation models, the dynamic safety distances based on ship types, and the impact of autonomous ships on heterogeneous traffic flows. The literature review is also orchestrated along these dimensions.

2.1. Traffic model

Traffic models serve as mathematical or computational representations designed to characterise and analyse traffic flows. They aid researchers in comprehending and prognosticating the behaviour and attributes of traffic flows. Based on scale, these models can be categorised into macroscopic, microscopic, and mesoscopic models. Macroscopic (e.g., Mohan and Ramadurai, 2013; Wang et al., 2022) models perceive traffic flow as a continuous fluid, concentrating solely on its aggregate characteristics such as flow, speed, and density, whilst

disregarding the nuances of individual vehicles. Such models typically employ differential or difference equations (Khan and Gulliver, 2018) to delineate the dynamics of traffic flow, with the Lighthill-Whitham-Richards (LWR) (Lighthill and Whitham, 1955) and Cell Transmission Model (CTM) (Daganzo, 1994) models being quintessential examples. Conversely, microscopic models view traffic flow as a discrete system constituted by individual vehicles. They focus on factors related to each vehicle's position, speed, acceleration, and driving behaviour, as well as the interactions between vehicles. The motion of individual vehicles in microscopic (Cardaliaguet and Forcadel, 2021) models is usually captured by car-following or lane-changing models, with the Intelligent Driver Model (IDM) (Treiber et al., 2000) and Minimizing Overall Braking Induced by Lane Changes (MOBIL) (Kesting et al., 2007) models being prominent examples. Mesoscopic models represent a hybrid approach, synthesising both macroscopic and microscopic models to portray traffic flow attributes across different spatial or temporal scales. This amalgamation ensures a balance between a holistic view and detailed insights. Multilevel or multi-resolution methods are typically employed in the construction of mesoscopic models, with examples including the three-tiered hybrid model (e.g., Storani et al., 2021; Jiang et al., 2020) and the multi-resolution hybrid simulation system (Son et al., 2022).

In the realm of maritime traffic research, scholars frequently draw inspiration from road traffic flow theories. Given the distinct characteristics of ships, such as their larger scale, comparatively slower velocities, and elongated reaction times, maritime traffic flow models are established to investigate the navigational efficiency of waterways. Initial studies on channel throughput capabilities typically utilised empirical formulas. Building on the spatial-temporal consumption theory, Liu et al. (2016) formulated a channel throughput capability computation model that accounts for the dynamic maritime domain. Gao et al. (2020) similarly leveraging the spatial-temporal consumption theory, probed into the ramifications of LNG ship navigation on the throughput capabilities of seaport channels. Liu et al. (2020) and collaborators, anchored in Automatic Identification System (AIS) data, analysed the traffic flow characteristics of ships entering and exiting ports. Employing the spatial-temporal consumption theory, they developed a maritime throughput computation model and forecasted channel throughput capabilities.

2.2. Traffic simulation model

In recent years, with the rapid advancement of computer simulation technology, scholars have shifted their focus towards employing computer simulation modelling techniques to study maritime traffic flow and port channel navigation efficiency. Some researchers have used simulation software or platforms such as AWESIM, MATLAB, ARENA (Dragović et al., 2017), FLEXSIM (Dulebenets et al., 2015), and WITNESS (Parola and Sciomachen, 2005) to study channel throughput capabilities via computer simulation. Uğurlu et al. (2014)) considering ship arrival patterns, developed a simulation model combining both docks and channels using the AWESIM simulation software. Their research delved into dock ship type, tonnage, berthing frequency, loading frequency, manoeuvring time, and transportation capacity. Almaz et al. (2006) utilizing the Arena simulation platform, pioneered the construction of the Istanbul Strait maritime traffic flow simulation model, which integrated various factors affecting safe passage through the strait. Legato and Mazza (2001) employed discrete event simulation using the Visual S. LAM simulation language to simulate the entire process of ship arrivals, berthing, and departures. Xin et al. (2019) grounded in AIS data, analysed the maritime traffic flow characteristics of the Xiazhimen channel and established a maritime traffic flow simulation model based on discrete event simulation.
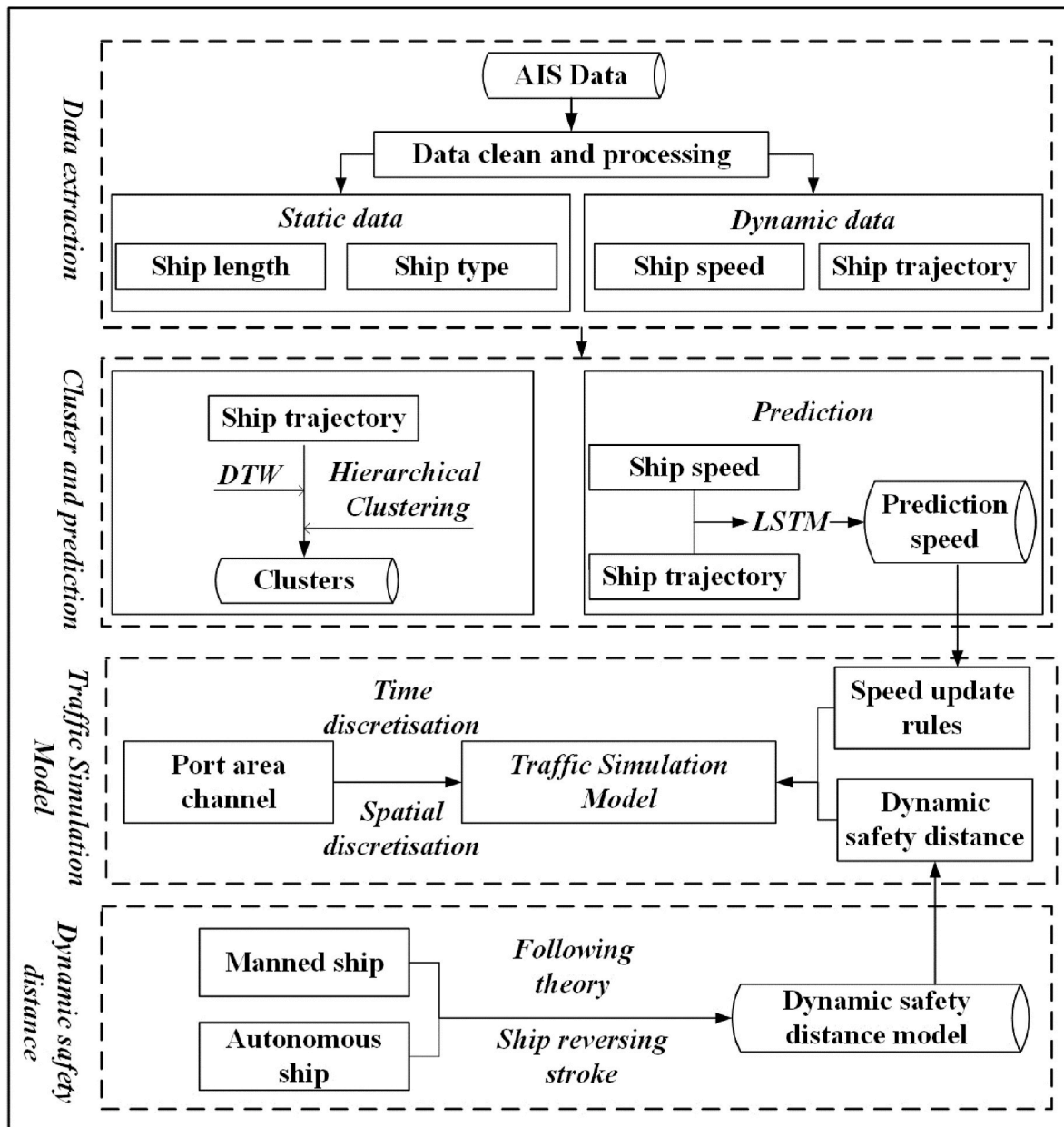
Fig. 1. Logical framework of the study.

2.3. Simulation model of ship traffic based on CA

At present, for waterway traffic, the majority of scholars have initiated the development of simulation models rooted in CA. Liu et al. (2010) drawing upon varying ship categories, safety distances, ship arrival patterns, and berth service levels, crafted a CA model for port waterway traffic flows. This model adeptly tackled the intricacies and non-linear challenges inherent in simulation. Subsequently, various researchers have integrated random variables into the CA framework during the simulation of ship traffic flows. This integration is to encapsulate the influence of environmental determinants on maritime manoeuvres, as delineated in works like Qi et al. (2017a, 2017b) and Qu and Meng (2012). Given the heightened activity within the approach channels, explorations into the ramifications of lane switching on traffic efficacy have been conducted, evident in studies such as Sun et al. (2015), Hu et al. (2017), and Qi et al. (2021). Jiang et al. (2019) introduced a sophisticated port waterway traffic simulation model, ingeniously integrating cellular automata with multi-agent systems.

This research meticulously examines the significant impact of ship behaviour on port operations, shedding light on the intricate dynamics and providing pivotal insights for enhancing operational efficiency and navigational safety within port precincts. Analogously, Liu et al. (2021) utilised both CA and multi-agent simulation paradigms to formulate a model that mimics the ingress and egress of Liquefied Natural Gas (LNG) carriers within ports.

2.4. Heterogeneous traffic flow modelling

Similarly, the heterogeneous traffic flow resulting from the introduction of autonomous driving vehicles first emerged on roads. With the development of autonomous driving technology, autonomous vehicles have begun to participate in traffic as main entities. As a result, the model of heterogeneous traffic flow (e.g., Tampere and van Arem, 2001; Hoogendoorn et al., 2014, Fagnant and Kockelman, 2015) has become a hot topic for researchers. Many researchers have investigated the impacts of Autonomous Vehicles (AVs) on the efficiency of road traffic

flow. Reza Mohajerpoor and his team used an analytical model to derive the expected traffic flow values and headway times for mixed autonomous and manually driven vehicles. Ye and Yamamoto (2018) leveraging the Two-State Safety Speed Model (TSM), established a dual-lane CA heterogeneous traffic flow model. This model incorporated both autonomous and conventional vehicles into the heterogeneous traffic flow to study the potential impacts of connected and autonomous vehicles on traffic flow. Guo et al. (2021) proposed a dual-queue mixed traffic flow model to describe the dynamics and flow conversions at intersections. Based on this mixed flow model, they developed a dynamic dual-layer framework to capture the behaviours and interactions of both manually driven and autonomous vehicles, enhancing the network performance of heterogeneous traffic flows. Yao et al. (2021) believed that autonomous vehicles following manually driven vehicles could lead to a decline in the performance of autonomous vehicles. Based on this, they derived and analysed the linear stability of heterogeneous traffic flows, considering the degradation of autonomous vehicles and the diversity of reaction times. Yang et al. (2022) developed a platoon cooperation strategy based on a "catch-up' mechanism, analyzing its impact on traffic dynamics within mixed environments. Zhang et al. (2023) enhanced a CA model to examine the characteristics of heterogeneous traffic, including electric vehicles. Xu et al. (2023) proposed a novel multi-view adaptive hierarchical spatial graph convolution network for predicting trajectories of varied traffic agents. Lastly, Ku et al. (2023) introduced an attention mechanism in graph construction neural networks, focusing on asymmetric spatiotemporal correlations in heterogeneous traffic, offering more sensitivity compared to traditional models.

According to the current research achievements, it's evident that within the prevailing traffic flow models, some have already incorporated the dynamic maritime safety distances. However, the primary focus of these models is on varying navigational behaviours of ships, neglecting the changes in safety requirements arising from alterations in speeds. Whilst road traffic models have begun emphasising heterogeneous traffic flows constituted by both autonomous and manually driven vehicles, maritime research predominantly centres on the situational awareness, intelligent collision avoidance, and route planning of autonomous ships. The theoretical and simulation models for heterogeneous ship traffic flow warrant further in-depth exploration.

3. Methodology

Studying heterogeneous traffic flow inclusive of autonomous ships is a complex and systematic endeavour. One of the primary datasets integrals to this research is the AIS data, which encompasses a plethora of both dynamic and static ship-related information, being crucial in navigation as ships transmit and receive these data. AIS data can be collected by satellite and received by shore-based base stations, which include ship identification information, Maritime Mobile Service Identities (MMSI) number, static information, and dynamic information, etc. Dynamic information includes a ship's position (longitude and latitude), heading, speed, bow direction, the ship's status, etc., while static information includes the ship's size, type, draught depth, destination, expected arrival time, etc. By analysing the AIS data, the historical trajectory, position change and speed change of the ship can be understood, and then the behavioural pattern of the ship and the speed change trend can be analysed. Therefore, our study begins with the processing and feature extraction of AIS data. Firstly, ships are categorised based on static data like their type and dimensions. Further classification ensues based on the pattern in their speed change, wherein the trajectories are grouped by speed characteristics. This process entails calculating trajectory similarity by speed attributes. The use of hierarchical clustering offers the benefit of a stratified data perspective without the prerequisite of specifying cluster numbers. Consequently, trajectories with analogous trends and attributes are grouped, furnishing requisite data for subsequent ship speed predictions.

For speed prediction, the LSTM model, renowned for its heightened sensitivity to spatiotemporal features in data, was employed. An LSTM network model was constructed hinged on velocity and positional data to forecast trajectory speeds exhibiting varying tendencies. This culminated in a speed control strategy. Following this, a dynamic safety distance computational model for both manned and autonomous ships was devised, grounded in car-following theories and suppositions regarding parameters of autonomous ships.

Conclusively, by integrating the speed control strategy and the dynamic safety distance computation into a CA-based simulation model, a heterogeneous maritime traffic flow simulation model was established, possessing a dual-speed control strategy. The logical framework of each segment is elucidated in Fig. 1.

3.1. Trajectory clustering based on velocity features

Before embarking on trajectory prediction, it is imperative first to undertake data pre-processing, trajectory similarity measurement based on velocity attributes, and subsequently trajectory clustering. These processes are instrumental in understanding the trends in ship speed variations and a broad categorisation within the targeted research area.

(1) Data pre-processing

In the data pre-processing stage, the main steps include the following: standardisation of the 'Speed', 'Lat', and 'Lon' columns of the data using the Z-Score (Al Shalabi et al., 2006) method, and elimination of outliers by excluding Z-Scores with absolute values greater than 3. The Z-Score is calculated using the formula:

$$Z = (X - \mu)/\sigma \tag{1}$$

where X is each observation, μ is the mean of the observations, and σ is the standard deviation of the observations.

After eliminating outliers, discontinuous trajectories are removed. Firstly, the time difference between two consecutive observations of the same MMSI is calculated, and then data points with too large time difference are removed. Finally, trajectories with lengths less than a certain spatial extent were filtered out. The latitude and longitude data were converted to distance data using the Haversine formula, which calculates the distance between two latitudes and longitudes. The formula is:

$$a = sin^2\left(\frac{\Delta\varphi}{2}\right) + \cos\varphi 1 * \cos\varphi 2 * sin^2\left(\frac{\Delta\lambda}{2}\right)$$
$$c = 2 * atan\,2\left(\sqrt{a}, \sqrt{(1-a)}\right) \tag{2}$$
$$d = R * c$$

where $\varphi 1$ and $\varphi 2$ represent the latitude of the first and the second point in radians, respectively.

$\Delta\varphi$ represents the difference between the latitudes of the two points in radians, calculated as $\varphi 2 - \varphi 1$, $\lambda 1$ and $\lambda 2$ represent the longitude of the first and the second point in radians, respectively, $\Delta\lambda$ represents the difference between the longitudes of the two points in radians, calculated as $\lambda 2 - \lambda 1$, R is the mean radius of the Earth (taking the value of 6371 km), a represent a helper variable in the formula, calculated using the latitudes and longitudes of the two points, c represent another helper variable, computed using the arctangent function applied to the square root of a and the square root of $1 - a$, d represent the final calculated distance between the two points on the surface of the sphere, in the same units as the radius R (usually km).

The process starts by finding the start point of each MMSI, then calculating the distances between the other points and this start point using the Haversine formula. These computed distances are subsequently added to the dataset as new features.

Before the similarity calculation, the trajectory data should be pre-processed again, the velocity of each ship trajectory is taken as a

Table 1
Pseudocode of trajectory clustering process.

Cluster Optimization
Input: Distance matrix D, Minimum number of clusters n_{min}, Maximum number of clusters n_{max}
1: for $n_{clusters}$ from n_{min} to n_{max} do
2:    linkage_matrix = linkage (D, method='ward')
3:    clusters = f_cluster (linkage_matrix, $n_{clusters}$, criterion='maxclust')
4:    score = silhouette_score (D, clusters, metric='precomputed')
5:    if score is better than best_score then
6:       best_score = score
7:       optimal_clusters = clusters
8:       optimal_number_of_clusters = $n_{clusters}$
9:    end if
10: end for
11: return optimal_clusters, optimal_number_of_clusters

sequence, and the distance of each sequence is split into segments of length $dist_{interval}$, and the average velocity of each segment is calculated. d denotes the sequence of distances, s denotes the sequence of velocities, and the new sequence of velocities, s' is computed in the following way:

$$s_i' = \begin{cases} \dfrac{\sum_{j:m_j \geq i \bullet dist_{interval} \ and \ m_j < (i+1)\bullet dist_{interval}} s_j}{count \ of \ j} & if \ count \ of \ j > 0 \\ \\ 0 & \\ & if \ count \ of \ j = 0 \end{cases} \quad (3)$$

where m_j is the jth element in the sequence of distances.

(2) Trajectory similarity metric

For similarity metric, the DTW algorithm is used to calculate the distance between two sequences (Zhang et al., 2023). Firstly, the data are grouped by MMSI, then the 'Dist' and 'Speed' values of each MMSI are combined into a two-dimensional array, finally, the DTW distance between each pair of data is calculated and the distance is stored in a two-dimensional array. The DTW algorithm excels at assessing the similarity between trajectories, exhibiting robustness with respect to time. It is capable of computing the distance between sequences of differing lengths, determining the distance between trajectories based on the correspondence of time-series features. Notably, DTW is free from parameter constraints and does not necessitate a one-to-one correspondence of time points. For a given sequence of d and s', of lengths n

and m, respectively, the DTW distance $D(d, s')$ can be calculated by the following recursive relation:

$$DTW(i,j) = dist(d|i|, s'|j|) + min \begin{cases} DTW(i, j-1) \\ DTW(i-1, j-1) \\ DTW(i-1, j) \end{cases} \quad (4)$$

where $DTW(i,j)$ is the DTW distance between $d[1 \cdots i]$ and $s'[1 \cdots j]$, $dist(\bullet, \bullet)$ is the Euclidean distance, and $D(m,n)$ is the final DTW distance.

(3) Clustering based on trajectory similarity

There are various clustering methods, including K-means (Son et al., 2022a; 2022b), Density-based spatial clustering of applications with noise (DBSCAN) and Hierarchical Clustering. In this study, the need to classify trajectories with similar speed change trends into the same category makes Hierarchical Clustering a more appropriate method.

Hierarchical clustering not only delivers the final clustering outcome but also offers a hierarchical perspective on the data. This method allows for a view of data clustering on varying levels of abstraction, transitioning from fine to coarse granularity, facilitating a deeper understanding of the similarities and disparities amongst the data. Unlike many clustering methods that require the pre-specification of the number of clusters to be formed, hierarchical clustering is devoid of this stipulation. The hierarchical structure and dendrogram facilitate a visual interpretation of clustering outcomes. It's adaptable, permitting the use of different distance metrics and linkage methods, thus making it flexibly applicable to diverse types of data and usage scenarios. Contrary to centroid-based clustering methods, hierarchical clustering negates the need to select initial centroids, which diminishes its sensitivity to initial conditions, thus consistently yielding stable results. Moreover, hierarchical clustering is amenable to both small and large samples. This is because it doesn't necessitate processing all data from the outset but builds clusters through progressive merging or division.

In the hierarchical clustering method, the ward method works to minimise the variance within each cluster by selectively merging the two clusters that minimise the variance of the total inner clusters at each step, whereas the *maxclust* criterion determines the final number of clusters by evaluating the inter- or intra-cluster distances or densities to determine the appropriate cut-off point (e.g., Li et al., 2022; Wang et al., 2021; Zhang et al., 2018). The precise merging of the ward method and the cut-off strategy of the *maxclust* criterion provides an ordered, multilevel clustering structure for the data.

The specific steps of hierarchical clustering include: 1) initialising the best contour score *best_score* and the corresponding number of clusters *best_num_clusters*, by iterating over a predefined range of different number of clusters $n_{clusters}$; 2) constructing the linkage matrix,
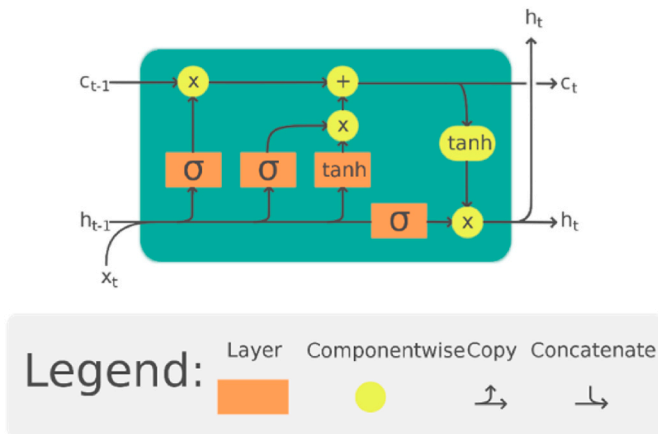
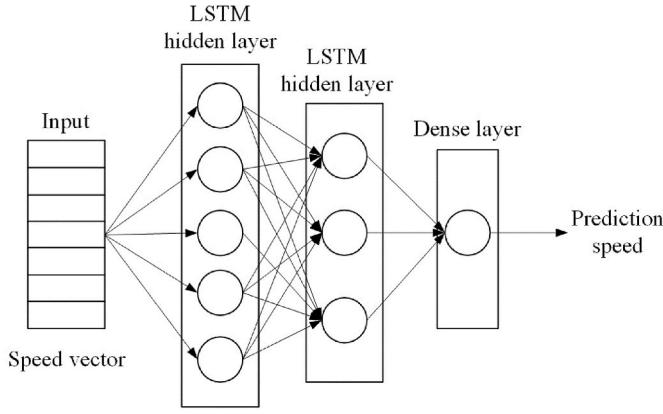**Fig. 2.** LSTM neuron structure diagram (Hochreiter and Schmidhuber, 1997)

Fig. 3. LSTM network structure diagram.

calculating the *linkage_matrix* using the *ward* method; 3) clustering the data according to the given number of clusters and the *maxclust* criterion, using the fast clustering *fcluster* method; 4) using the pre-computed *distance* matrix distance and the clustering result *clusters* to compute the profile score *score*, and 5) after iterations, using the *best_num_clusters* to reconstruct the linkage matrix and form the final *clusters*.

For a given distance matrix D and a range of number of clusters $n_{min} \leq n_{clusters} \leq n_{max}$, the process of trajectory clustering is shown in Table 1.

During the iteration process, for each $n_{clusters}$, the number of clusters that maximises the profile score is chosen as the final optimal number of clusters.

3.2. LSTM-based ship speed prediction

LSTM (Fig. 2) networks are particularly adept at predicting speed using ship trajectory data. The inherent ability of LSTM to capture and remember information over extended time periods is crucial for analysing long-term dependencies in time-series data like trajectories. Its capability to handle sequences of varying lengths and its inherent adaptability make it ideal for processing spatial-temporal data, which often consists of trajectories or event sequences of diverse lengths. Moreover, the LSTM's contextual memory ensures a more profound comprehension of patterns and relationships within sequences, especially in the realm of spatial-temporal data. It is sensitive to time-space features, effectively capturing correlations in temporal and spatial dimensions, which is invaluable for analysing and predicting trends and patterns in such data. Furthermore, its flexibility in processing multi-dimensional inputs allows for a holistic understanding by integrating time-series data with other attributes.

In this study, a LSTM neural network model was used to predict the speed corresponding to every 60 m in the trajectory. The data contained multiple ship trajectories, each containing information such as longitude, latitude, timestamp, and distance from the starting point to the current point. The prediction goal is to predict the current velocity based on the current location and its previous velocity.

First, a one-dimensional interpolation process was performed on each trajectory to ensure that there was a data point every 60 m. The raw data were transformed into new data at 60 m/data point to obtain a more continuous trajectory.

$$Dist_{new} = \text{interp1d} (Dist, Speed, Time, axis = 0) \quad (5)$$

For the input data of the neural network model, the distance to starting point and the interpolated speed were selected as features and these two features were normalised, i.e., the mean was subtracted and divided by the standard deviation to transform it into a normal distribution with mean 0 and variance 1. For the output of the model, the interpolated speed was selected and was also normalised similarly.

$$x_{norm} = \frac{x - x_{min}}{x_{max} - x_{min}} \quad (6)$$

An LSTM model containing a 50-neuron LSTM layer, and a fully connected layer of output neurons was used (Fig. 3). The Adam optimiser (Kingma and Ba, 2014) was chosen, as well as the mean square error as the loss function. During model training, one group of trajectories was selected as the validation set for monitoring the model performance during training, and the other group as the training set. The maximum number of epochs for model training was set to 200, and an early stopping strategy was also introduced, i.e., if the loss in the validation set did not decrease further after 10 consecutive epochs, the model training would be ended early. At the same time, the parameters of the model were saved after each epoch, and if it was found that the new model was not better than the previous one, it would not overwrite the previously saved model.

The equations provided describe the mathematical formulations underpinning the LSTM neural network, a specialized type of Recurrent Neural Network (RNN) renowned for its proficiency in learning temporal dependencies in sequential data. The LSTM architecture comprises various components such as forget, input, and output gates, along with cell and hidden states, each playing a pivotal role in governing the network's learning process. The specified equations can be delineated as follows:

$$
\begin{aligned}
f_t &= \sigma_g \left(W_f \cdot [h_{t-1}, x_t] + b_f \right) \\
i_t &= \sigma_g \left(W_i \cdot [h_{t-1}, x_t] + b_i \right) \\
\widetilde{C}_t &= \tanh \left(W_C \cdot [h_{t-1}, x_t] + b_C \right) \\
C_t &= f_t \cdot C_{t-1} + i_t \cdot \widetilde{C}_t \\
o_t &= \sigma_g \left(W_o \cdot [h_{t-1}, x_t] + b_o \right) \\
h_t &= o_t \cdot \tanh \left(C_t \right)
\end{aligned}
\quad (7)
$$

where f_t, i_t, o_t are the activation values of the oblivion gate, the input gate, and the output gate, C_t is the cell state, and $\widetilde{C}_t$ represents the candidate memory cell state. This state contains the information that could potentially be added to the long-term state C_t at the current time step. h_t is the hidden state, x_t is the input, and σ_g is the sigmoid activation function. W_f, W_f, W_C, and W_o are the weight matrices associated with the forget gate, input gate, cell state, and output gate, respectively. b_f, b_i, b_C and b_o are the bias vectors for the corresponding gates and cell state.

For a Fully Connected layer (FC), the output is as follows:

$$y = W \bullet h + b \quad (8)$$

where h represents the input features or activations from the preceding layer. The matrix W and vector b are the weight and bias parameters of the layer, respectively, which are learned during the training of the neural network. The dot product $W \bullet h$ signifies the weighted sum of the input features and adding the bias b to this sum introduces an additional degree of freedom to the model, allowing it to better fit the training data. The resultant y typically undergoes a non-linear activation function before being forwarded to subsequent layers, aiding the network in learning complex patterns and representations from the input data.

3.3. Dynamic ship safety distance based on the follow theory

For ships of diverse classifications, the prerequisites for maintaining safety distances are subject to variations, contingent upon distinct velocities and environmental conditions. This complexity is accentuated in the evolving landscape of maritime traffic, where heterogeneity is not merely a function of scale and type but also encompasses a shift towards a composite structure of both manned and autonomous ships. In such a diversified framework, the heterogenous characteristics of distinct ships and their corresponding safety requisites become increasingly
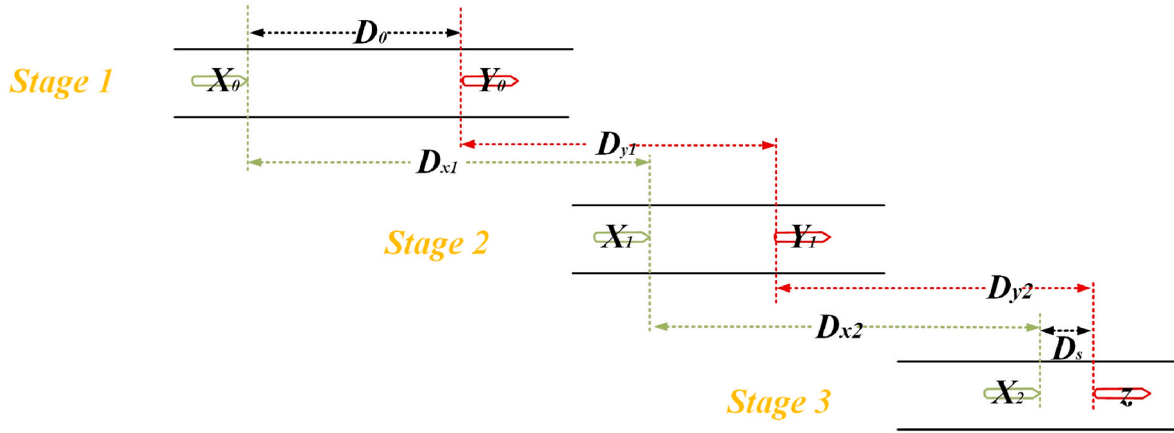
Fig. 4. Schematic diagram of ship following behaviour.

prominent and intricate, necessitating nuanced considerations and strategies to address the dynamic environment of maritime navigation and safety in the forthcoming era.

Current methods for calculating the safe distance of ships primarily focus on car-following theory and ship domain. In restricted channels, the value of a ship's domain is generally 5–7 times the length of the ship, and the methods of determining this value have evolved from earlier Fujii models (1971), Goodwin observational data models (1975), and others (e.g., Szlapczynski and Szlapczynska, 2017; Yang et al., 2023), to ship domain models based on mathematical analysis and AIS data. This study adopts a safety distance of five times the ship's length, a parameter consistent with practices in restricted channels and supported by theoretical models like Goodwin's. This choice is informed by the specific navigational characteristics of the Tianjin Port main channel and aligns with the evolution of ship domain methods from Fujii's early model to recent AIS data-based analyses.

Following theory can characterise the generation and evolution process of traffic flow and can depict the following behaviour of heterogeneous ship flow in busy traffic conditions. Hence, in this study, a method based on the car-following behaviour of ships to calculate dynamic safety distance is employed.

The ship following behaviour model divides the ship's reaction to an emergency braking situation into three stages (Fig. 4.).

Stage I : The leading ship Y encounters an emergency and begins to reverse and brake, while the following ship X continues to sail at its original speed.

Stage II: The following ship X receives the dynamics of the leading ship Y's reversing and braking through VHF and begins to reverse and brake accordingly.

Stage III: The following ship X completes its braking and maintains a certain safety distance, denoted as D_S , from the leading ship Y, which has already completed its braking.

If the start time of the braking manoeuvre of the front ship is taken as a reference, the distance D_Y between the initial position of the front ship and the rear ship at the completion of braking can be calculated by the following formula:

$$D_Y = D_0 + D_{y1} + D_{y2} \tag{9}$$

where $D_{y1} + D_{y2}$ is the braking distance of the front ship; D_0 represents the net distance before the two ships before the front ship is performing the braking manoeuvre.

The rear ship X receives the ship dynamics of the forward ship Y braking in reverse via VHF, and the distance D_{x1} travelled forward before starting to perform the reverse braking is also called the reaction distance, and if it is assumed that D_{x2} is the distance travelled by the rear

Table 2
Correspondence between tonnage, length, and power of ships.

Ship type	Ship length(m)	Power (kW)
Oil ships	$8.491DWT^{0.291}$	$(6809 + 0.0896DWT)*0.746$
Cargo ships	$7.945DWT^{0.301}$	$(7617 + 0.081DWT)*0.746$
Container ships	$4.089DWT^{0.380}$	$(0.863DWT-1905)*0.746$
Miscellaneous cargo ship	$6.839DWT^{0.321}$	$(748 DWT+0.552DWT)*0.746$

ship in the process of braking to the expected speed, the following formula can be used for the calculation of the rear ship's distance of travel, D_X, after the forward ship has braked:

$$D_X = D_{x1} + D_{x2} \tag{10}$$

where $D_{x1} = Vt$, V represents the sailing speed of the rear ship when the front ship takes braking manoeuvre; t represents the reaction time of the rear ship, which consists of the reaction time of the driver and the braking action time of the main engine.

In order to maintain the full safety of the two ships during braking, the distance between the two after the completion of braking should be greater than the safety margin D_s, i.e., $D_Y - D_X \geq D_s$. Based on the above conditions, the following formula for the safe longitudinal distance between ships can be determined:

$$D_0 \geq D_{x1} + D_{x2} + D_s - D_y \tag{11}$$

where $D_y = D_{y1} + D_{y2}$ represents the braking distance of the front ship.

D_{x2} and D_y are the reversing strokes of the front and rear boats respectively, and the reversing strokes can be calculated by the following empirical formulae:

$$S = \frac{1}{2}\frac{Wk}{gT_p}V^2 \tag{12}$$

where S represents reversing stroke (m); g is acceleration of gravity (9.8 m/s²); W represents ship's displacement (t); k represents ship's forward direction of the virtual mass coefficient, taken as 1.07; T_p represents propeller reversing pull (t), taken as 0.01 M_P, M_P represents the reversing power; V represents the ship's speed during reversing motion (m/s).

Assuming a normal following situation, the relationship between the ship's safety distance and speed obtained from the above equation has:

$$D_0 = D_{x1} + D_s + \frac{V_x^2 kW_X}{2gT_{PX}} - \frac{V_y^2 kW_Y}{2gT_{PY}} \tag{13}$$

As delineated in Table 2, some correspondence is established between ship length and Deadweight Tonnage (DWT), as well as between ship power and DWT, in accordance with the Design Code of General
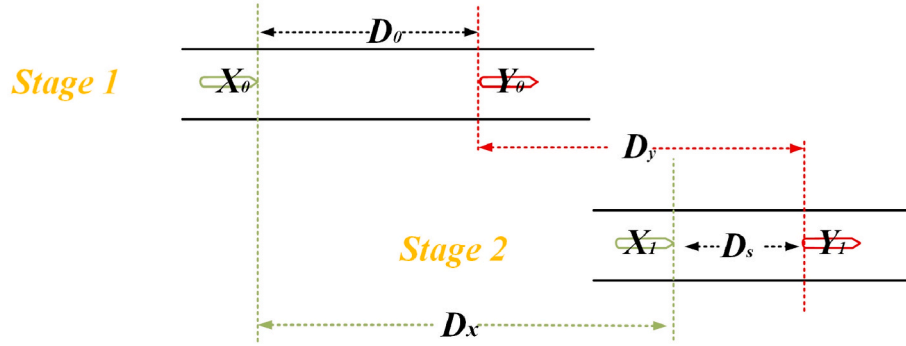
Fig. 5. Schematic diagram of the following behaviour of an autonomous ship.

Layout for Sea Ports.[2] This correspondence is derived through rigorous statistical analysis and regression conducted on an extensive array of ship parameters. It is noteworthy that the relationship between ship length and DWT is characterised by an exponential correlation, whilst the association between ship power and DWT is distinctly proportional.

Regarding the assumptions made in our dynamic safety distance model for autonomous ships, we have assumed that in the future maritime Internet of Things environment, autonomous ships will be able to obtain real-time information about surrounding ships and promptly act upon it. Under this premise, autonomous ships are more sensitive to the speed changes of the ships ahead compared to manned ships. In the dynamic safety distance model, we can thus omit the time taken to acquire information about speed changes of the leading ship and the time for the ship's own reaction and operation.

The fundamental sequence underlying the following behaviour of an autonomous ship mirrors that of a manned ship; however, a distinctive variance emerges in the decision-making dynamics, accounting for these assumptions. An autonomous ship is endowed with the capability to instantaneously discern and respond to the deceleration of the preceding ship, thereby abbreviating the reaction process depicted as stage 2 in Fig. 4. This enhanced sensitivity and real-time responsiveness effectively reduce the necessary safety distance, as reflected in the optimized formula (Eq. 14) compared to the computation for manned ships (Eq. (13)). Consequently, the following behaviour of such autonomous ships, including their decision-making dynamics and the calculation of dynamic safety distance, is aptly represented in Fig. 5. This refined model and the adaptations in computational methodologies underscore the nuanced differences and advancements in autonomous maritime navigation.

$$D_0 = D_s + \frac{V_x^2 k W_X}{2g T_{PX}} - \frac{V_y^2 k W_Y}{2g T_{PY}} \tag{14}$$

3.4. Simulation model of ship traffic flow based on CA

The CA model, when applied to ship traffic flow simulation, stands out due to its blend of precision, adaptability, and efficiency. Drawing inspiration from the Na-Sch rules and tailoring it to the maritime domain, the CA model offers a keen reflection of real-world ship movements, allowing for granular control over ship behaviours. Its inherent scalability ensures real-time simulation of ship generation patterns and the dynamic safety distances resulting from ship interactions. Moreover, by integrating modules based on predicted speeds, the model can implement ship speed control strategies, further aligning simulations with actual traffic conditions. In essence, the CA model's adaptability and holistic approach render it invaluable for portraying and understanding complex maritime traffic dynamics.

(1) Location update rules

The ship's location update follows the rules shown in Eq. (18).

$$x_n(t+1) = x_n(t) + v_n(t) \tag{15}$$

(2) Calculation of dynamic safety distance

During navigation, the distance between the target ship n and the nearest leading ship $n+1$ is first calculated. If the target ship is a manned ship, d_{safe} is calculated according to Eq. (13); if the target ship is autonomous ship, d_{safe} is calculated according to Eq. (14). If the distance between the following ship and the leading ship is greater than the safe distance, i.e., $x_{n+1}(t) - x_n(t) > d_{safe}$, then the ship enters the acceleration rule; otherwise, it enters the deceleration rule.

(3) Acceleration rules:

For situations where the predicted speed strategy v_{data} exists:

a. Calculate the speed difference: $\Delta v = v_{data} - v_n$.
b. If $\Delta v > 0$, then accelerate: $v_n = v_n + min\{\Delta v, a\}$, where a is the pre-set acceleration.
c. If $\Delta v < 0$, then decelerate: $v_n = v_n - min\{\Delta v, a\}$.

For situations where the speed strategy v_{data} does not exist, acceleration is carried out according to part (a), but not exceeding the maximum speed: $v_n \rightarrow min\{v_n + a, v_{max}\}$, where v_{data} represents the speed of the ship according to predictions, and $v_{data}(x)$ represents the predicted speed at position x.

(4) Deceleration rules

When the distance between $ship_n$ and $ship_{n+1}$ is less than the pre-set safe distance, $x_{n+1} - x_n < d_{safe}$, the rear ship needs to slow down as Eq. (16).

$$v_n \rightarrow min\{v_n(t) - 1, v_{min}\} \tag{16}$$

4. Case study

Tianjin Port, as a large and busy port in northern China, carries an important role as a freight distribution centre. The main channel of Tianjin Port, as the main channel for ships to enter and leave the port, carries an irreplaceable important role, which has a good research value. Thus, the main channel of Tianjin Port was selected as a study case. It was discretised according to the requirements of the cellular automaton model, and the visualization effect is shown in Fig. 6.
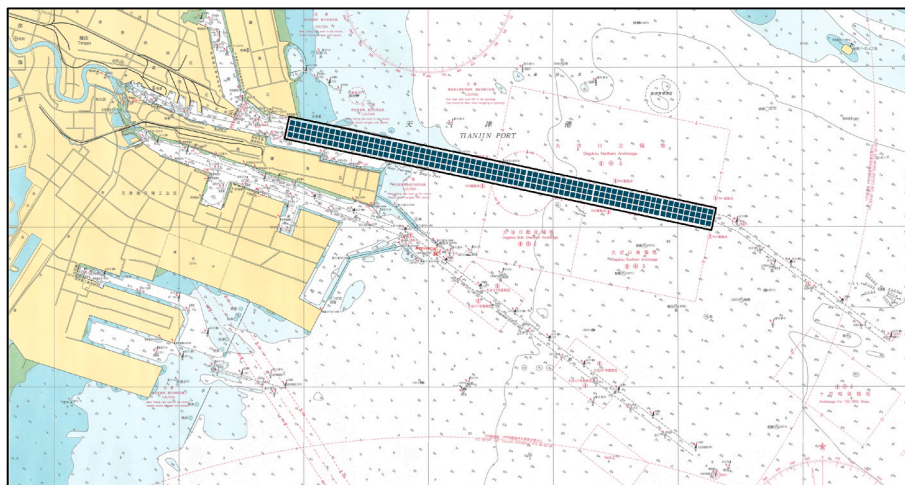
---

[2] JTS 165–2013, Design Code of General Layout for Sea Ports, People's Communications Press, Beijing, 2013.
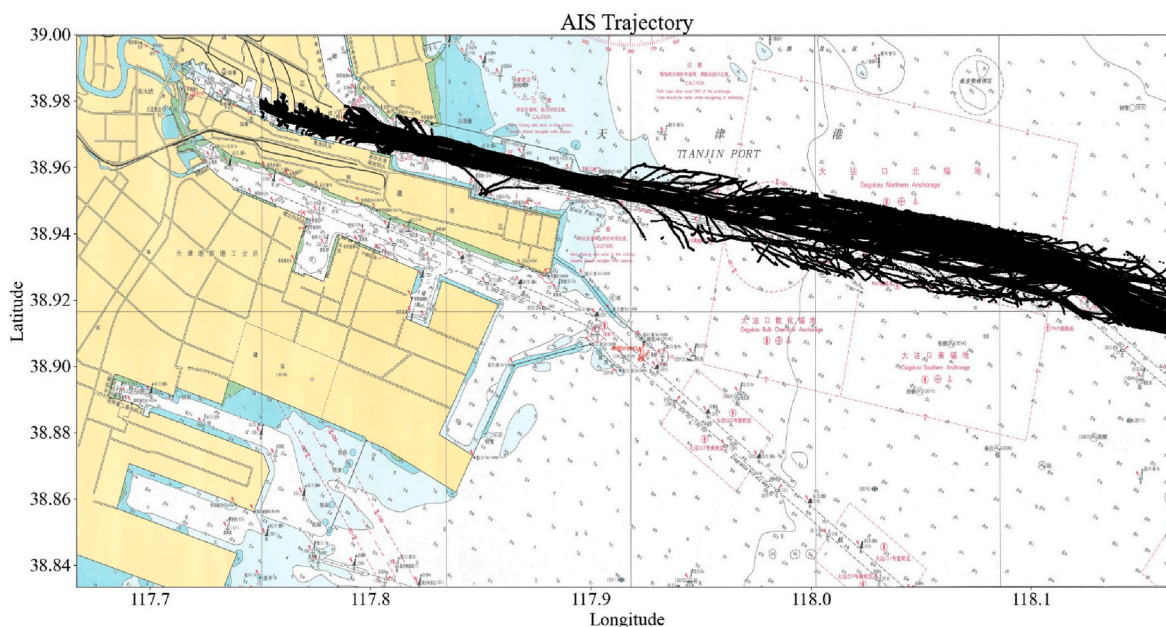
Fig. 6. Range of target waters.

Fig. 7. Ship trajectory in Tianjin Port main channel.

4.1. Traffic flow feature extraction

The AIS data of the main channel of Tianjin Port from 1 July to July 30, 2019 were selected as the dataset (Fig. 7). By analysing the ship types and ship sizes, it can be found that the proportion of cargo ships has reached 94.3%, of which the proportion of ships with a length of <180 m, 180–300 m and >300 m is about 1:7:2 (Fig. 8). Therefore, these three types of cargo ships are mainly considered for trajectory clustering and velocity prediction.

According to the clustering results (Fig. 9), the trajectories can be classified into three categories according to the velocity trend, and the training and prediction of the three categories are carried out respectively to obtain the result in Fig. 10. Mean Squared Error (MSE), Mean Absolute Error (MAE), and Mean Absolute Percentage Error (MAPE) were employed as evaluation metrics for our study. The results, as presented in Table 3, demonstrate that the accuracy of our predictions is over 90%. This high level of accuracy substantiates the effectiveness of our predictive model.

In response to the observed deviations in ship speed predictions, particularly regarding the higher speed deviation in Type 3 ships (over 300 m) compared to Type 2 ships (240 m), it is important to consider the unique characteristics of the Tianjin Port main channel used in our study. Typically, larger ships are expected to have more stable speed patterns, theoretically making them easier to predict accurately. However, the Tianjin Port main channel presents unique navigational challenges due to specific convergence points, which can lead to speed variations that deviate from conventional expectations. In addition, ships during navigation are significantly influenced by the speed of vessels ahead, particularly in dense traffic scenarios. These specific conditions have influenced the predictive results, leading to higher speed deviations for larger ships in our dataset, as they adjust their speeds in response to the movements of preceding ships.

After transforming the position information into metric spatial order, a new two-dimensional array is formed with the corresponding predicted velocities to obtain the velocity control strategy based on the predicted data.
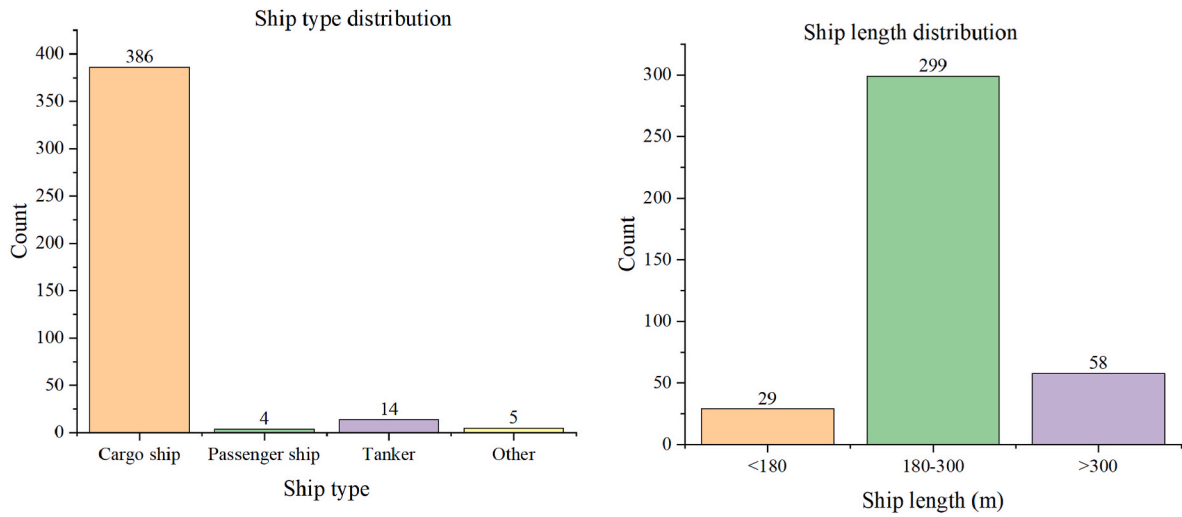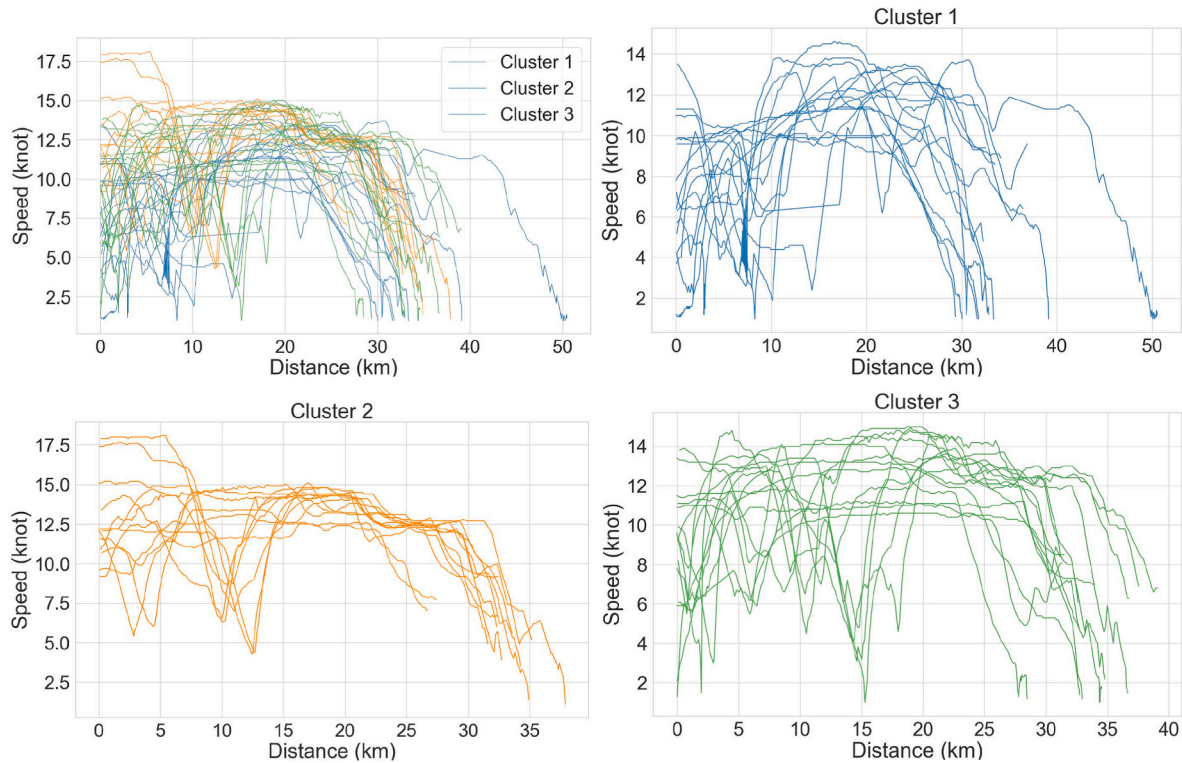
Fig. 8. Ship Type and ship length distribution.

Fig. 9. Ship trajectory clustering.

4.2. Parameter setting

a. Temporal discretisation and spatial discretisation of the simulation

According to the spatial-temporal discretisation requirements of the theoretical model of the CA and the actual traffic conditions of the main channel of Tianjin Port, the size of each cell is set to represent a space of 15 × 15 m, and each time step t represents 30s, and the whole channel is discretised into a cellular space of 60 × 2000, and the ship moves forward one cell when sailing at the speed of 1kn for one time step, which

facilitates the movement of the ship in the whole system.

According to the provisions in the Classification Code for Steel Sea-going Ships,[3] the reversing power should not be less than 70 per cent of the forward power and the reversing speed should not be less than 50 per cent of the forward speed (Table .4).

b. Simulation background settings based on AIS data

From the AIS data analysis (July 1, 2019–July 7, 2019), we categorised ships as <180 m, 180–300 m, and >300 m, with a generation

---

[3] China Classification Society. Classification Code for Steel Sea-going Ships. Beijing: China Classification Society, 2023.
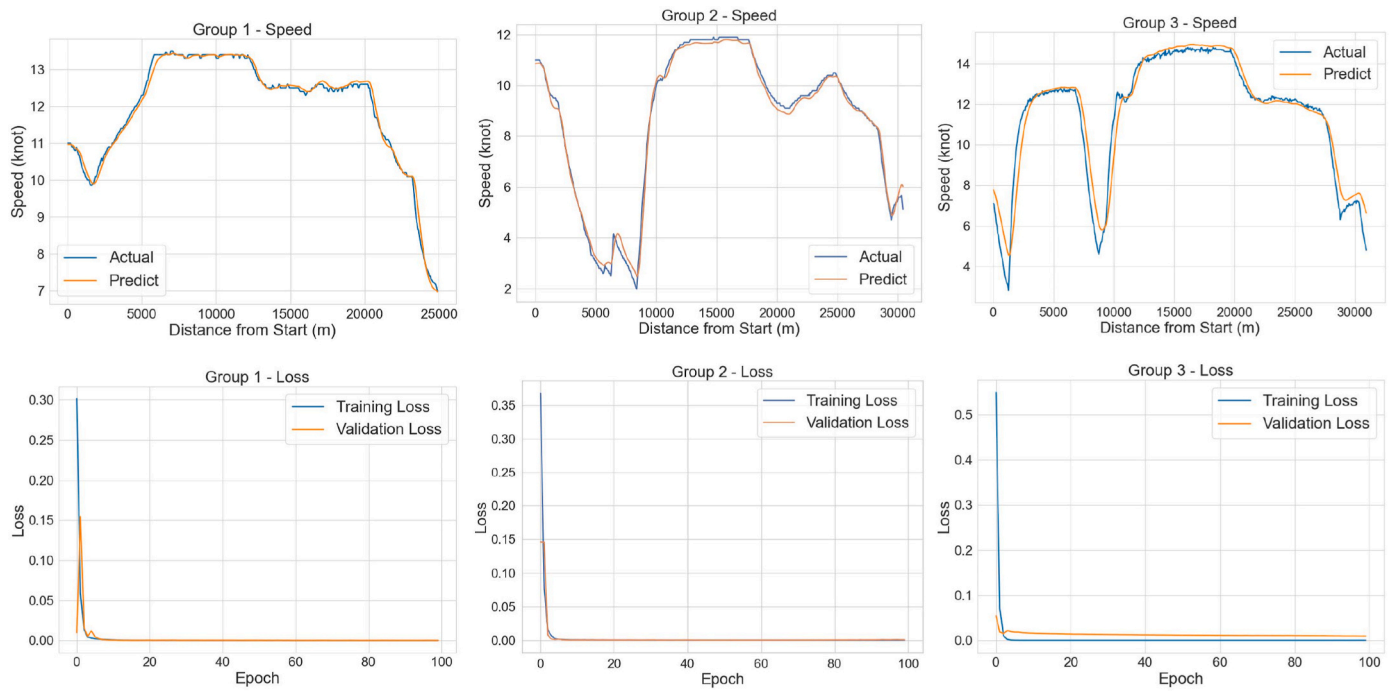
Fig. 10. Velocity prediction with loss function variation.

Table 3
Error analysis.

Indicators	Group 1	Group 2	Group 3
MSE	0.029	0.165	0.564
MAE	0.116	0.262	0.489
MAPE	1.056%	4.785%	6.252%

Table 4
Cargo ship parameters.

Ship length(m)	DWT(t)	Ship's main engine power P (kW)	Ship reversing power M_P (kW)
180	34,185	7610	5327
240	82,833	10,696	7487
300	173,871	16,206	11,344
Autonomous ship	82,833	10,696	7487

Table 5
Definition of ship types.

Type1	Type2	Type3	Type4	Type5	Type6
<180 m	180–240 m	>300 m	Autonomous ship <180 m	Autonomous ship 180–240 m	Autonomous ship >300 m

ratio of 1:7:2. To facilitate precise dynamic safety distance calculations, these categories refined to specific lengths of 180 m, 240 m, and 300 m. This approach aligns with the statistical distribution and enhances the model's accuracy and practicality. The time interval between the arrival of ships at the beginning of the channel is counted as 60min. For a simple description, manned ships and autonomous ships are defined as shown in Table 5.

4.3. Model verification

To verify the effectiveness of the simulation model and the speed control strategy, simulations were carried out without increasing the traffic flow density and without adding the dynamic safety distance calculation module.

Upon examination of the trajectory and variations in a ship's speed, it becomes evident that despite the third group in Fig. 11 manifesting a prediction error marginally larger than its preceding two counterparts, the devised simulation model retains the capacity to emulate a more authentic trend of the ship's speed alterations, particularly in scenarios characterised by sparse traffic density. Given that the principal objective of this investigation revolves around elucidating the ramifications of alterations in ship behaviour, specifically acceleration and deceleration, on traffic efficiency, it is inferred that a traffic model proficient in simulating the trend of speed changes fulfils the fundamental prerequisites to facilitate the progression of the subsequent phases of this study.

4.4. Experiment and analysis

Three groups of experiments were carried out respectively, and the length of time for each set of experiments was 24 h. The first group was without dynamic safety distance, and the ships were navigated according to a fixed safety distance. The second group added the calculation of dynamic safety distance in the simulation, and the safety distance was calculated according to the scale and speed of the ships before and after at every step. The third group added a certain proportion of autonomous ships based on the addition of the calculation of dynamic safety distance. The main difference is that autonomous ships have a smaller safety distance compared to manned ships.

4.4.1. Scenario 1: increase in traffic flow

This simulation scenario increases the density of ship traffic flow to simulate future heavy traffic due to increased demand for ships entering and leaving the port, while a fixed safety distance is set based on five times the length of the ship to observe the ship following behaviour in the trajectory (Fig. 12).
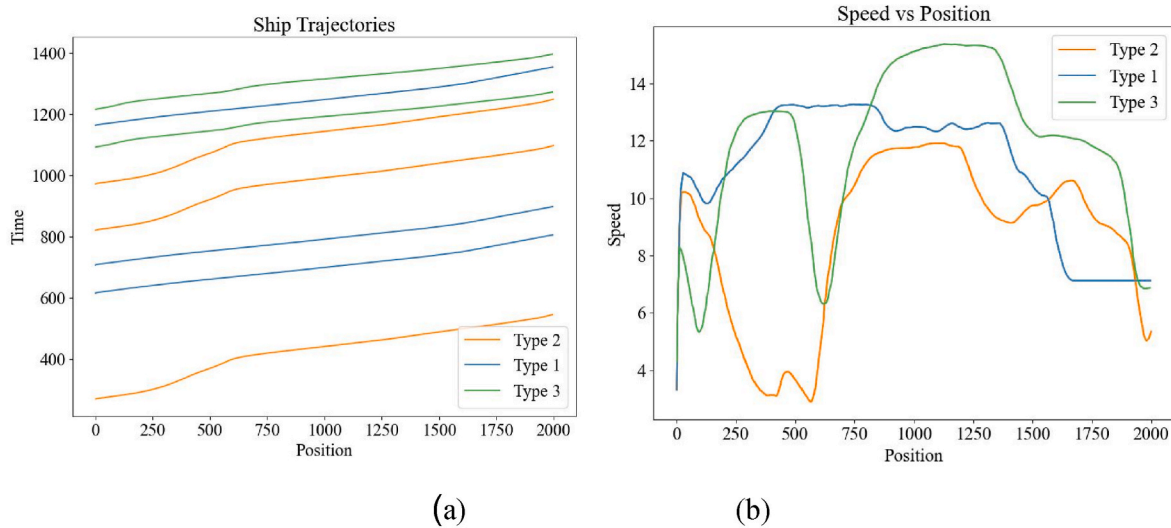
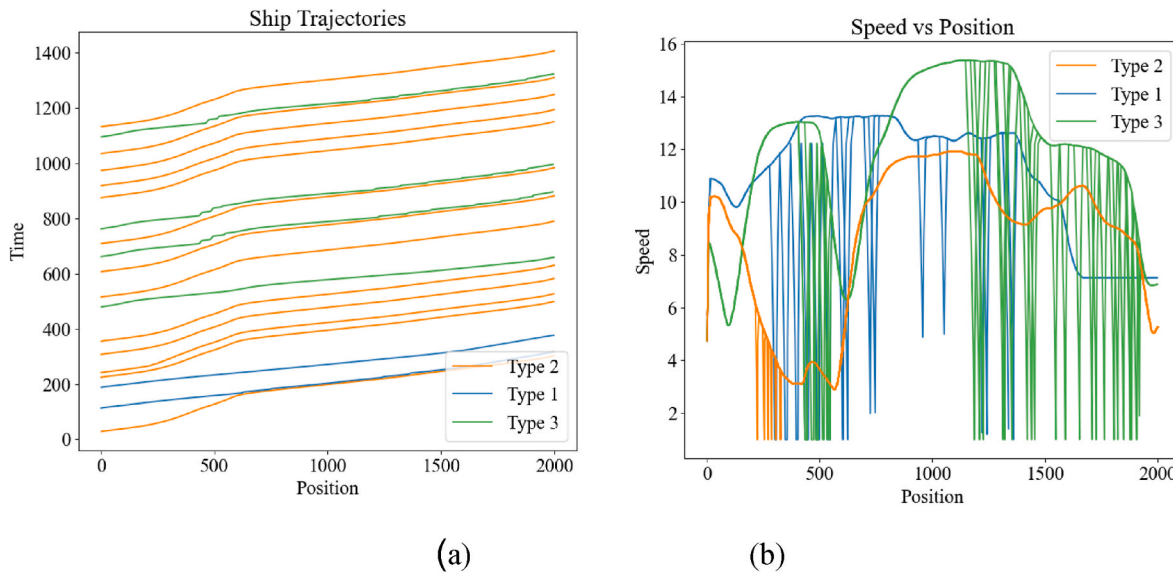**Fig. 11.** Experimental results for verification: (a) ship trajectory, and (b) speed versus position.

Fig. 12. Experimental results after increasing the density of traffic flow: (a) ship trajectory, and (b) speed versus position.

Table 6
Result of increasing traffic density.

Ship type	Type1	Type2	Type3
Ship number	3.700 ± 0.786	9.800 ± 1.826	3.200 ± 1.618
Average speed (knot)	9.375 ± 0.672	7.160 ± 0.044	9.510 ± 0.596

To quantitatively analyse the experiment, avoid random error caused by computer, 10 groups of experiments were carried out to obtain the number of ships and average speed of different types of ships completing the voyage, and the average of the results of the ten groups was taken, and the results shown in Table 6.

An examination of the trajectory and speed change trends derived from the experimental results reveals that under conditions of high traffic flow density, ship n tends to exhibit deceleration behaviours. This is necessitated by the imperative to maintain a predetermined safety distance from the preceding ship. Subsequent to achieving this safety distance, additional deceleration is mandated by the speed control strategy, culminating in a series of frequent deceleration and accelera-

tion behaviours throughout the navigation process. This pattern is vividly depicted in Fig. 12, contributing to augmented energy consumption by the ship and a concomitant diminution in traffic efficiency during actual navigation.

4.4.2. Scenario 2: incorporation of a dynamic safety distance calculation module

With the addition of the dynamic safety distance module, it is evident that the ship's speed fluctuates less and the average speed is higher than before , The need for ships to slow down to a minimum speed to maintain a safe distance is greatly reduced (Fig. 13). The mean of the results of the ten groups of experiments shown in Table 7.

From the experimental results, it can be found that the number of ships completing the voyage has shown a small increase, and the average speed of ships has also shown a small increase, which indicate that the introduction of dynamic safety distance can improve the efficiency of ship traffic. The increase in speed is mainly observed in the ships with a length of 180 m and 300 m, and the increase in the number of ships passing through is mainly observed in the ships with a length of 240 m. The total number of ship passages was 17.8, with an increase of 6.5%,
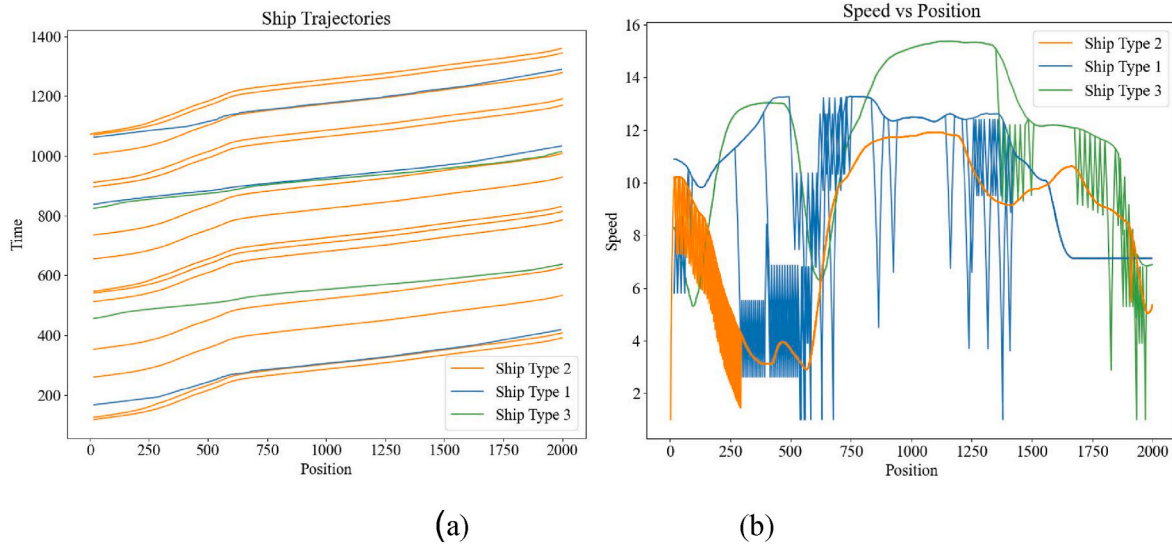
Fig. 13. Experimental results after incorporation of a dynamic safety distance calculation module: (a) ship trajectory, and (b) speed versus position.

Table 7
Result of incorporation of dynamic safety distance.

Ship type	Type1	Type2	Type3
Ship number	3.700 ± 1.872	10.100 ± 3.035	4.000 ± 1.155
Average speed (knot)	9.600 ± 0.350	7.170 ± 0.022	10.003 ± 0.373

and the average speed was increased by 2.5%.

4.4.3. Scenario 3: accession of 10%–100% autonomous ships with dynamic safety distance

Upon integrating autonomous ships, we undertook ten experimental sets spanning from 10 % to 100 % of the total traffic flow. Each set was replicated 10 times, during which we measured the mean velocity of each ship type and the average number of voyages completed. Furthermore, for every experimental set, the proportion of the traffic flow was designated, as delineated in Table 8.

We selected representative trajectory plots (Fig. 14) and velocity trend graphs (Fig. 15) from each experimental set for consolidation and analysis. It can be observed that concerning the traffic trajectories, as the proportion of autonomous ships within the total traffic flow increases, there is a gradual augmentation in traffic density. In terms of velocity trends, the frequency of ships undergoing substantial acceleration and deceleration appears to be diminishing.

By analysing the number of ships that completed their voyages (Table 9), it becomes evident that as the proportion of autonomous ships rises, the number of ships completing their journeys within the

stipulated experimental duration also progressively increases. This corroborates the hypothesis that autonomous ships positively influence the channel's throughput capacity.

As the proportion of autonomous ships increases, we observe a gradual decrease in the magnitude of acceleration and deceleration for all ship types. This trend, illustrated in Fig. 14, is attributable to the advanced capabilities of autonomous ships in our model. These ships are designed to detect changes in the speed of the ships ahead and react more promptly compared to traditional ships. As a result, they can adjust their speed earlier and more smoothly, reducing the need for abrupt speed changes. This leads to a smoother traffic flow and less pronounced velocity fluctuations. The improved reaction time and decision-making of autonomous ships, as modelled, not only enhance navigational efficiency but also contribute to safer and more predictable maritime traffic patterns.

In addition to analysing the number of voyages completed by the ships, we delved into the effects of an increasing proportion of autonomous sailing ships on the average speed of each type of ship in every experimental set. Fig. 16 delineates the average speed outcomes from ten experiments for different ship types, alongside the corresponding standard deviations. Notably, the speeds of Type 2 and Type 5 ships remain relatively stable, showing little to no variance with the increase in the proportion of autonomous ships. Conversely, the average speeds of the remaining ship types tend to incrementally rise as the proportion of autonomous sailing ships increases. This phenomenon can be attributed to the fact that, due to their speed control strategies, Type 2 and Type 5 ships maintain lower speeds, thus rarely finding themselves

Table 8
Experimental working condition setting.

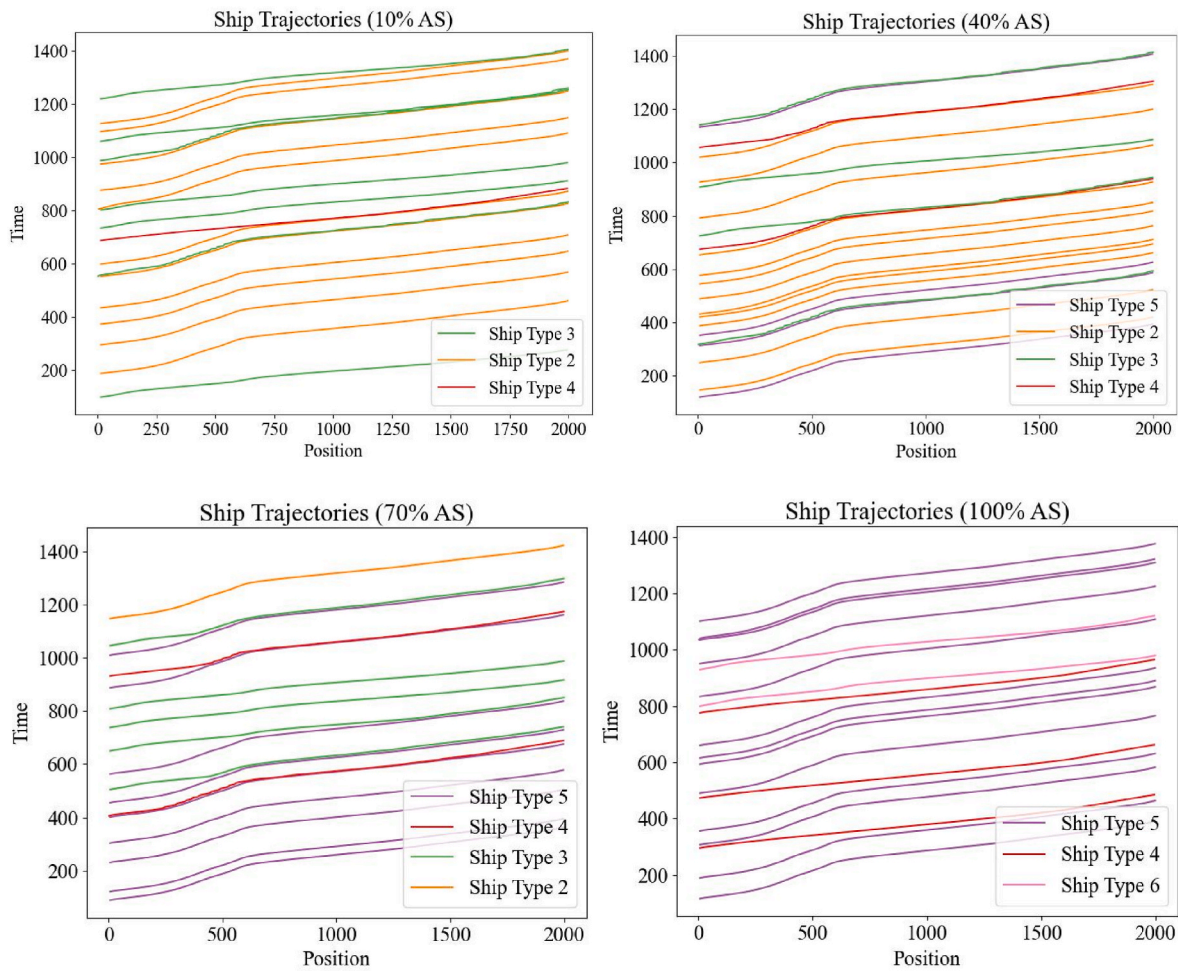| AS proportions | Ship type | | | | | |
	Type1 (manned)	Type2 (manned)	Type3 (manned)	Type4 (AS)	Type5 (AS)	Type6 (AS)
10%	–	70%	20%	10%	–	–
20%	–	60%	20%	10%	10%	–
30%	–	50%	20%	10%	20%	–
40%	–	40%	20%	10%	30%	–
50%	–	30%	20%	10%	40%	–
60%	–	20%	20%	10%	50%	–
70%	–	10%	20%	10%	60%	–
80%	–	–	20%	10%	70%	–
90%	–	–	10%	10%	70%	10%
100%	–	–	–	10%	70%	20%

*AS: Autonomous Ships.

Fig. 14. Traffic flow trajectories with the inclusion of autonomous ships.

nearing ships ahead of them. Meanwhile, other ship types, with their average speeds surpassing those of Type 2 and Type 5 ships, necessitate frequent deceleration and acceleration actions, especially in dense traffic scenarios. Consequently, these ships exhibit heightened sensitivity to speed variations as the proportion of autonomous ships shifts.

4.5. Discussion

With the rapid advancement of smart ship technologies, the maritime future will inevitably comprise a heterogeneous traffic flow, co-inhabited by both autonomous and manned ships. Owing to their digital and informational prowess, autonomous ships excel in swiftly and precisely acquiring navigational situations and surrounding environmental data compared to their manned counterparts. This imparts them with a distinctive advantage in navigation efficiency and economic viability. Against this backdrop, this study delved into the impact of autonomous ships on the efficiency of heterogeneous traffic flow.

This investigation particularly considered the incorporation of dynamic safety distances and the capability of autonomous ships to rapidly decide and execute in the face of evolving navigational situations. Based on the experimental results shown in Fig. 17, some observation and consideration are as follows.

a. When ships are positioned at distances shorter than a predetermined safety threshold, they predominantly maintain a reduced speed to uphold the safety distance. Such a practice substantially augments fuel consumption, hampers maritime traffic efficiency, and escalates transportation costs. Nonetheless, the introduction of dynamic safety

distances seems poised to mitigate these challenges, to enhance traffic efficiency.
b. The integration of autonomous ships optimises the dynamic safety distances between ships, leading to more stable speed alterations when confronted with changing traffic situations.
c. Both the inclusion of dynamic safety distances and autonomous ships bolster the navigational efficiency of waterway traffic systems. The impact of autonomous ships is especially pronounced: when their proportion reaches 100%, the overall pass-through efficiency witnesses an uplift of 26.35%.

The experimental results demonstrate that the proposed model effectively simulates the impact of incorporating dynamic safety distances on the characteristics of heterogeneous traffic flow. Additionally, the results reflect how changes in the proportion of autonomous ships affect the efficiency of heterogeneous traffic flows. The outcomes align with objective patterns, thus validating the effectiveness and advancement of the model.

Drawing upon our literature review, we note that most existing heterogeneous traffic flow models differentiate between manned and autonomous vehicles, with discussions primarily centred around road traffic (e.g., Yang et al., 2022; Zhang et al., 2023; Zheng et al., 2020). However, research focusing on the distinct characteristics and developmental trends of heterogeneous traffic flows comprising manned and autonomous ships is relatively scarce. Our model contributes to this underexplored area by enriching the study of waterway traffic dynamics, particularly in the context of the gradual shift towards autonomous navigation. This not only enhances the current understanding of
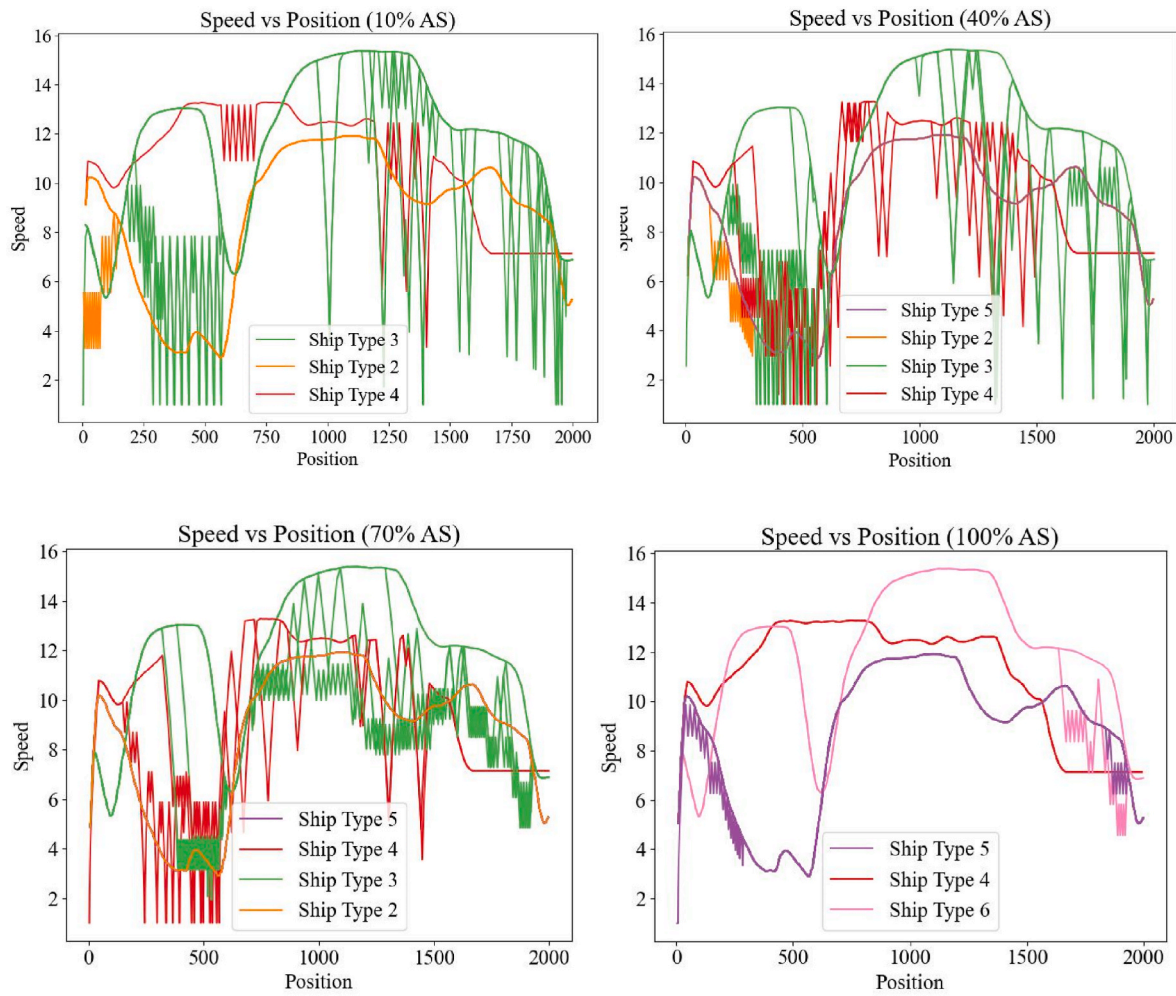
Fig. 15. Traffic flow trajectories with the inclusion of autonomous ships.

Table 9
Statistics on the number of ships completing the voyage.

AS proportions	Ship type				
	Type2 (manned)	Type3 (manned)	Type4 (AS)	Type5 (AS)	Type6 (AS)
10%	12.400 ± 2.261	4.200 ± 2.267	2.300 ± 0.816	–	–
20%	10.800 ± 1.327	4.500 ± 1.432	1.900 ± 0.539	1.800 ± 0.600	–
30%	9.900 ± 1.155	4.000 ± 0.875	1.900 ± 0.875	3.800 ± 1.499	–
40%	7.400 ± 1.685	3.700 ± 1.487	3.000 ± 1.095	5.800 ± 1.249	–
50%	4.000 ± 1.100	4.700 ± 1.414	3.900 ± 0.875	7.400 ± 1.333	–
60%	3.700 ± 1.900	5.100 ± 0.943	3.300 ± 0.900	8.100 ± 2.022	–
70%	2.300 ± 0.816	4.700 ± 2.708	2.700 ± 1.750	10.800 ± 2.409	–
80%	–	4.700 ± 1.616	3.100 ± 0.700	12.700 ± 2.648	–
90%	–	2.000 ± 0.471	3.200 ± 1.397	13.400 ± 1.563	2.222 ± 0.629
100%	–	–	3.700 ± 2.114	12.700 ± 3.830	4.700 ± 2.5728

*AS: Autonomous Ships.

maritime traffic flow but also lays a foundational framework for future research in the progressive evolution of waterway traffic towards autonomous navigation.

5. Conclusion

This paper employs hierarchical clustering to categorise trajectories with similar speed variation features and utilises LSTM models to predict ship speeds, forming a speed control strategy based on predictive data, which is novel in traffic simulation modelling. Moreover, extending from the principles of following-theory, models have been developed to compute dynamic safety distances for both manned and autonomous ships. This innovation propels the refinement of maritime traffic simulation models in terms of safety. Further, a port waterway simulation model based on CA has been developed, integrating data-driven speed control strategies while maintaining dynamic safety distances, resulting in a comprehensive simulation model with dual speed control mechanisms.

From the experimental results, one can observe that dynamic safety distance requirements can diminish the frequency with which ships undertake significant deceleration and acceleration manoeuvres. Furthermore, the efficiency of maritime port transport is considerably influenced by speed strategies. The integration of autonomous sailing ships affects different ship types in varied ways. For ships which inherently maintain a slower pace, they tend to persist with their languid speeds. However, for the swifter ships, the incorporation of autonomous sailing ships can further amplify the efficiency. When the
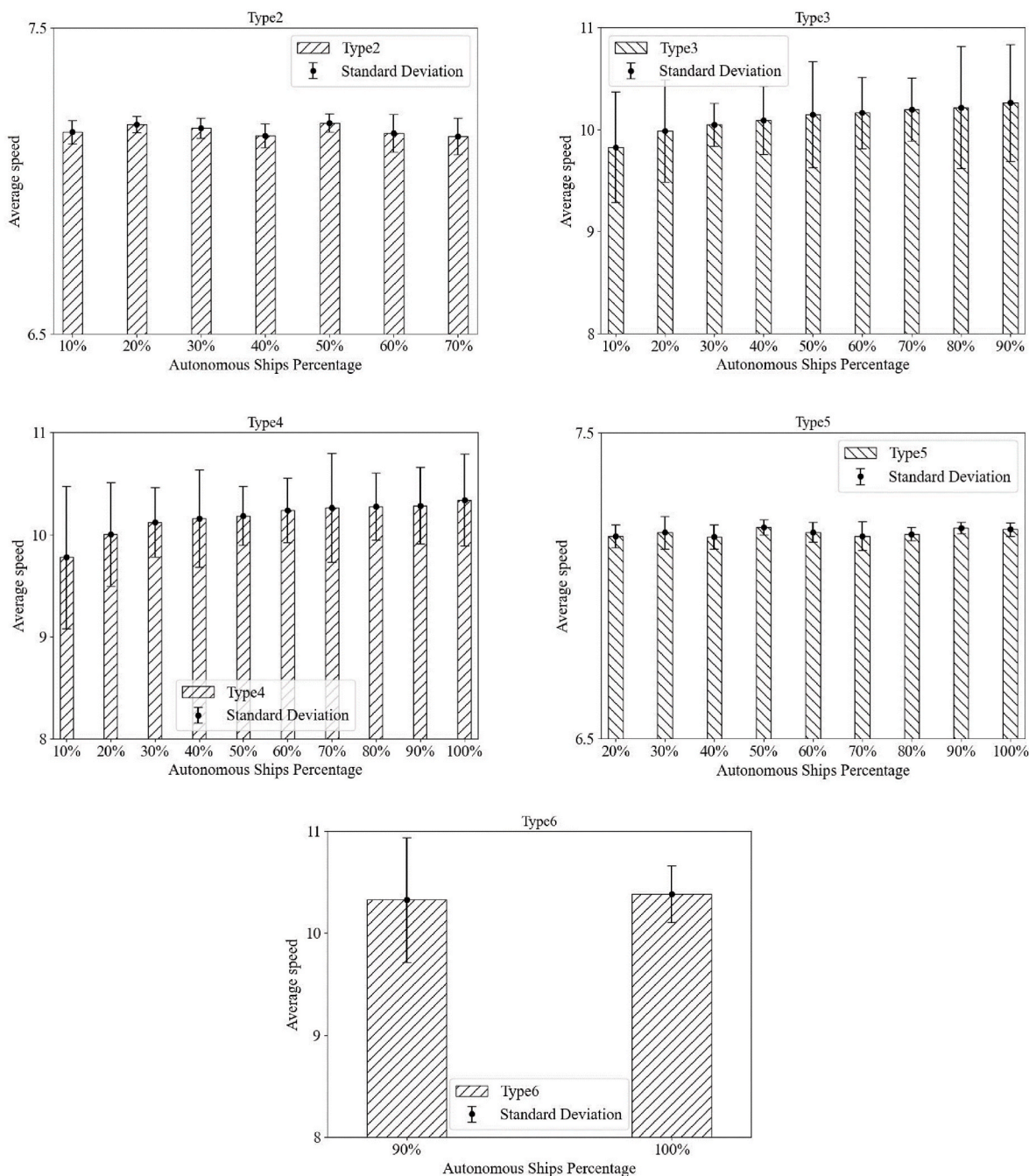
Fig. 16. Change in average ship speed with increasing proportion of autonomous ships.

proportion of autonomous ship reaches 100%, the overall pass-through efficiency witnesses an uplift of 26.35%.

An accurate model for ship traffic efficiency assessment plays a pivotal role in supporting maritime authorities with waterway planning, traffic organization, and safety oversight, thereby positively influencing the growth and efficient operation of ports. The model introduced in this study enriches the theoretical foundation of maritime traffic flow and offers novel perspectives on quantifying the efficiency of heterogeneous traffic. However, the current model necessitates a significant number of parameter inputs with a high demand for precision, resulting in a relatively intricate computational process. Future research will focus on further optimising and refining the model's parameter input. Furthermore, this study's reliance on data specific to the Tianjin Port main channel presents a limitation, potentially impacting the model's broader

applicability. Future investigations should incorporate a more varied dataset, thereby extending the model's relevance to diverse maritime settings. The proposed dynamic safety distance model is suitable for both uni-directional and bi-directional heterogeneous traffic flows, requiring specific modifications tailored to the particular navigational conditions of each scenario.

CRediT authorship contribution statement

Yang Liu: Formal analysis, Methodology, Writing – original draft. **Jingxian Liu:** Conceptualization, Funding acquisition, Supervision. **Qian Zhang:** Methodology, Supervision, Writing – review & editing. **Yi Liu:** Conceptualization, Resources. **Yukuan Wang:** Data curation, Validation.
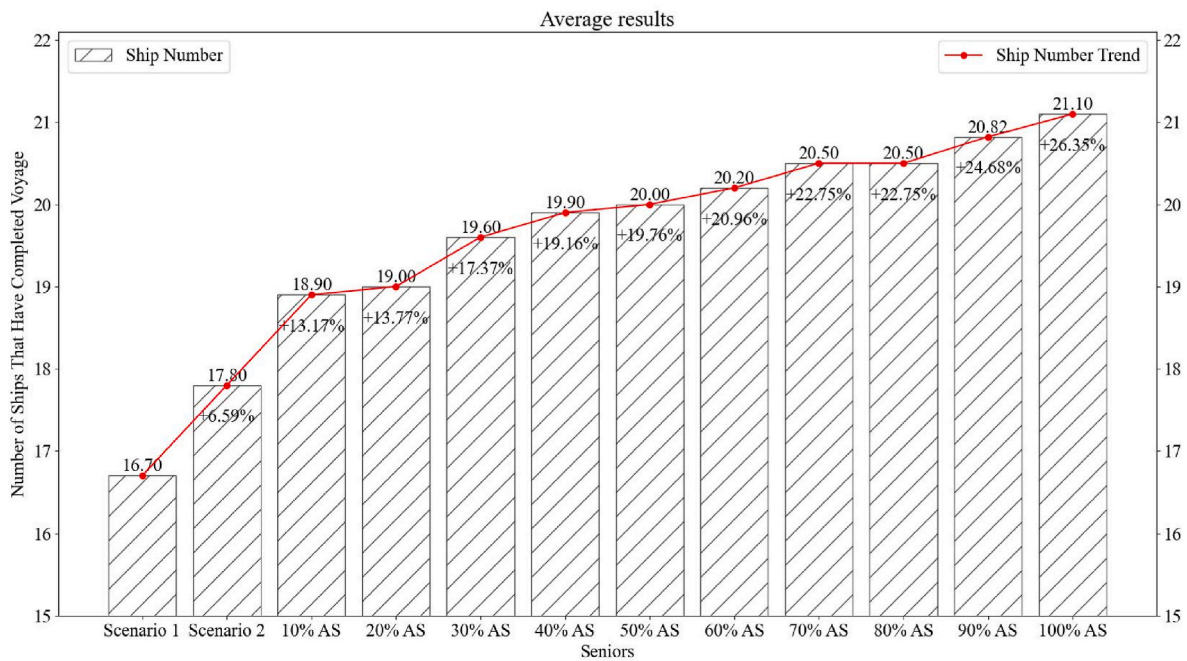
Fig. 17. Statistics on number of ships passed: average results of 10 experiments.

Declaration of competing interest

The authors declare that they have no known competing financial interests or personal relationships that could have appeared to influence the work reported in this paper.

Data availability

The data that has been used is confidential.

References

Al Shalabi, L., Shaaban, Z., Kasasbeh, B., 2006. Data mining: a preprocessing engine. J. Comput. Sci. 2 (9), 735–739.

Almaz, A.O., Or, I., Ozbas, B., 2006. Investigation of transit maritime traffic in the strait of Istanbul through simulation modeling and scenario analysis. International Journal of Simulation 7 (7), 1–9.

Cardaliaguet, P., Forcadel, N., 2021. From heterogeneous microscopic traffic flow models to macroscopic models. SIAM J. Math. Anal. 53 (1), 309–322. https://doi.org/10.1137/20M1314410.

Daganzo, C.F., 1994. The cell transmission model: a dynamic representation of highway traffic consistent with the hydrodynamic theory. Transp. Res. Part B Methodol. 28 (4), 269–287. https://doi.org/10.1016/0191-2615(94)90002-7.

Dragović, B., Tzannatos, E., Park, N.K., 2017. Simulation modelling in ports and container terminals: literature overview and analysis by research field, application area and tool. Flex. Serv. Manuf. J. 29, 4–34.

Dulebenets, M.A., Golias, M.M., Mishra, S., Heaslet, W.C., 2015. Evaluation of the floaterm concept at marine container terminals via simulation. Simulat. Model. Pract. Theor. 54, 19–35. https://doi.org/10.1016/j.simpat.2015.02.008.

Fagnant, D.J., Kockelman, K., 2015. Preparing a nation for autonomous vehicles: opportunities, barriers and policy recommendations. Transport. Res. Pol. Pract. 77, 167–181. https://doi.org/10.1016/j.tra.2015.04.003.

Fujii, Y., Tanaka, K., 1971. Traffic capacity. J. Navig. 24 (4), 543–552. https://doi.org/10.1017/S0373463300022384.

Gao, X., Chen, L., Chen, P., Luo, Y., Mou, J., 2020. Capacity analysis for approach channels shared by LNG carriers. J. Mar. Sci. Eng. 8 (9), 697. https://doi.org/10.3390/jmse8090697.

Goodwin, E.M., 1975. A statistical study of ship domains. J. Navig. 28 (3), 328–344. https://doi.org/10.1017/S0373463300041230.

Guo, Q., Ban, X.J., Aziz, H.A., 2021. Mixed traffic flow of human driven vehicles and automated vehicles on dynamic transportation networks. Transport. Res. C Emerg. Technol. 128, 103159 https://doi.org/10.1016/j.trc.2021.103159.

Hoogendoorn, R., van Arerm, B., Hoogendoom, S., 2014. Automated driving, traffic flow efficiency, and human factors: literature review. Transport. Res. Rec. 2422 (1), 113–120. https://doi.org/10.3141/2422-13.

Hochreiter, S., Schmidhuber, J., 1997. Long short-term memory. Neural Comput. 9 (8), 1735–1780.

Hu, H., Chen, X., Sun, Z., 2017. Effect of water flows on ship traffic in narrow water channels based on cellular automata. Pol. Marit. Res. 24, 130–135. https://doi.org/10.1515/pomr-2017-0115. S3 (95).

Jiang, J., Dellaert, N., Van Woensel, T., Wu, L., 2020. Modelling traffic flows and estimating road travel times in transportation network under dynamic disturbances. Transportation 47, 2951–2980.

Jiang, L., Huang, G., Huang, C., Wang, W., 2019. Data mining and optimization of a port vessel behaviour behavioural model under the Internet of Things. IEEE Access 7, 139970–139983. https://doi.org/10.1109/ACCESS.2019.2943654.

Kingma, D.P., Ba, J., 2014. Adam: a method for stochastic optimization. arXiv preprint arXiv:1412.6980. https://doi.org/10.48550/arXiv.1412.6980.

Khan, Z.H., Gulliver, T.A., 2018. A macroscopic traffic model for traffic flow harmonization. European Transport Research Review 10 (2), 1–12. https://doi.org/10.1186/s12544-018-0291-y.

Kesting, A., Treiber, M., Helbing, D., 2007. General lane-changing model MOBIL for car-following models. Transport. Res. Rec. 1999 (1), 86–94. https://doi.org/10.3141/1999-10.

Ku, Y., Guo, C., Zhang, K., Cui, Y., Shu, H., Yang, Y., Peng, L., 2023. Toward directed spatiotemporal graph: a new idea for heterogeneous traffic prediction. IEEE Intelligent Transportation Systems Magazine. https://doi.org/10.1109/MITS.2023.3315329.

Li, H., Lam, J.S.L., Yang, Z., Liu, J., Liu, R.W., Liang, M., Li, Y., 2022. Unsupervised hierarchical methodology of maritime traffic pattern extraction for knowledge discovery. Transport. Res. C Emerg. Technol. 143, 103856 https://doi.org/10.1016/j.trc.2022.103856.

Lin, J., Diekmann, P., Framing, C.E., Zweigel, R., Abel, D., 2022. Maritime environment perception based on deep learning. IEEE Trans. Intell. Transport. Syst. 23 (9), 15487–15497. https://doi.org/10.1109/TITS.2022.3140933.

Lighthill, M.J., Whitham, G.B., 1955. On kinematic waves II. A theory of traffic flow on long crowded roads. Proc. Roy. Soc. Lond. Math. Phys. Sci. 229 (1178), 317–345. https://doi.org/10.1098/rspa.1955.0089.

Liu, J., Zhou, F., Li, Z., Wang, M., Liu, R.W., 2016. Dynamic ship domain models for capacity analysis of restricted water channels. J. Navig. 69 (3), 481–503.

Liu, C., Liu, J., Zhou, X., Zhao, Z., Wan, C., Liu, Z., 2020. AIS data-driven approach to estimate navigable capacity of busy waterways focusing on ships entering and leaving. Ocean. Eng. 218, 108215 https://doi.org/10.1016/j.oceaneng.2020.108215.

Legato, P., Mazza, R.M., 2001. Berth planning and resources optimisation at a container terminal via discrete event simulation. Eur. J. Oper. Res. 133 (3), 537–547. https://doi.org/10.1016/S0377-2217(00)00200-9.

Liu, J., Zhou, F., Wang, M., 2010. Simulation of waterway traffic flow at harbor based on the ship behavior and cellular automata. In: 2010 International Conference on Artificial Intelligence and Computational Intelligence, vol. 3. IEEE, pp. 542–546. https://doi.org/10.1109/AICI.2010.352.

Liu, J., Liu, Y., Qi, L., 2021. Modelling liquefied natural gas ship traffic in port based on cellular automaton and multi-agent system. J. Navig. 74 (3), 533–548. https://doi.org/10.1017/S0373463321000059, 2021.

Mohan, R., Ramadurai, G., 2013. State-of-the art of macroscopic traffic flow modelling. Int. J. Adv. Engin. Sci. Applied Mathem. 5, 158–176. https://doi.org/10.1007/s12572-013-0087-1.

Parola, F., Sciomachen, A., 2005. Intermodal container flows in a port system network:: analysis of possible growths via simulation models. Int. J. Prod. Econ. 97 (1), 75–88. https://doi.org/10.1016/j.ijpe.2004.06.051.

Qi, L., Zheng, Z., Gang, L., 2017a. Marine traffic model based on cellular automaton: considering the change of the ship's velocity under the influence of the weather and sea. Phys. Stat. Mech. Appl. 480–494. https://doi.org/10.1016/j.physa.2017.04.125.

Qi, L., Zheng, Z., Gang, L., 2017b. A cellular automaton model for ship traffic flow in waterways. Phys. Stat. Mech. Appl. 471, 705–717. https://doi.org/10.1016/j.physa.2016.12.028.

Qu, X., Meng, Q., 2012. Development and applications of a simulation model for vessels in the Singapore Straits. Expert Syst. Appl. 39 (9), 8430–8438. https://doi.org/10.1016/j.eswa.2012.01.176.

Qi, L., Ji, Y., Balling, R., Xu, W., 2021. A cellular automaton-based model of ship traffic flow in busy waterways. J. Navig. 74 (3), 605–618. https://doi.org/10.1017/S0373463320000636, 2021.

Schröder-Hinrichs, J.U., Song, D.W., Fonseca, T., Lagdami, K., Shi, X., Loer, K., 2019. Transport 2040: Automation, Technology, Employment-The Future of Work. World Maritime University, Transport, 2040.

Storani, F., Di Pace, R., Bruno, F., Fiori, C., 2021. Analysis and comparison of traffic flow models: a new hybrid traffic flow model vs benchmark models. European Transport Res. Rev. 13 (1), 1–16. https://doi.org/10.1186/s12544-021-00515-0.

Son, S., Qiao, Y.L., Sewall, J., Lin, M.C., 2022. Differentiable hybrid traffic simulation. ACM Trans. Graph. 41 (6), 1–10. https://doi.org/10.1145/3550454.3555492.

Son, W.J., Cho, I.S., 2022a. Development of collision risk assessment model for bridge across waterways based on traffic probability distribution. Ocean Eng. 266, 112844 https://doi.org/10.1016/j.oceaneng.2022.112844.

Son, W.J., Cho, I.S., 2022b. Analysis of trends in mega-sized container ships using the K-means clustering algorithm. Appl. Sci. 12 (4), 2115. https://doi.org/10.3390/app12042115.

Sun, Z., Chen, Z., Hu, H., Zheng, J., 2015. Ship interaction in narrow water channels: a two-lane cellular automata approach. Phys. Stat. Mech. Appl. 431, 46–51. https://doi.org/10.1016/j.physa.2015.02.079.

Szlapczynski, R., Szlapczynska, J., 2017. Review of ship safety domains: models and applications. Ocean Eng. 145, 277–289. https://doi.org/10.1016/j.oceaneng.2017.09.020.

Tampere, C., van Arem, B., 2001. Traffic flow theory and its applications in automated vehicle control: a review. Proceedings of IEEE Intelligent Transportation Systems 391–397. https://doi.org/10.1109/ITSC.2001.948689.

Treiber, M., Hennecke, A., Helbing, D., 2000. Congested traffic states in empirical observations and microscopic simulations. Phys. Rev. 62 (2), 1805. https://doi.org/10.1103/PhysRevE.62.1805.

Uğurlu, O., Yüksekyıldız, E., Köse, E., 2014. Simulation model on determining of port capacity and queue size: a case study for BOTAS Ceyhan Marine Terminal. TransNav: Int. J. Marine Navig. Safety of Sea Transp. 8 (1) https://doi.org/10.12716/1001.08.01.16.

Veitch, E., Alsos, O.A., 2022. A systematic review of human-AI interaction in autonomous ship systems. Saf. Sci. 152, 105778 https://doi.org/10.1016/j.ssci.2022.105778.

Wang, Y., Yu, X., Guo, J., Papamichail, I., Papageorgiou, M., Zhang, L., et al., 2022. Macroscopic traffic flow modelling of large-scale freeway networks with field data verification: state-of-the-art review, benchmarking framework, and case studies using METANET. Transport. Res. C Emerg. Technol. 145, 103904 https://doi.org/10.1016/j.trc.2022.103904.

Wang, L., Chen, P., Chen, L., Mou, J., 2021. Ship AIS trajectory clustering: an HDBSCAN-based approach. J. Mar. Sci. Eng. 9 (6), 566. https://doi.org/10.3390/jmse9060566.

Xin, X., Liu, K., Yang, X., Yuan, Z., Zhang, J., 2019. A simulation model for ship navigation in the "Xiazhimen" waterway based on statistical analysis of AIS data. Ocean Eng. 180, 279–289. https://doi.org/10.1016/j.oceaneng.2019.03.052.

Xu, D., Shang, X., Peng, H., Li, H., 2023. MVHGN: multi-view adaptive hierarchical spatial graph convolution network based trajectory prediction for heterogeneous traffic-agents. IEEE Trans. Intell. Transport. Syst. https://doi.org/10.1109/TITS.2023.3248090.

Yang, X., Zou, Y., Chen, L., 2022. Operation analysis of freeway mixed traffic flow based on catch-up coordination platoon. Accid. Anal. Prev. 175, 106780 https://doi.org/10.1016/j.aap.2022.106780.

Yao, Z., Xu, T., Jiang, Y., Hu, R., 2021. Linear stability analysis of heterogeneous traffic flow considering degradations of connected automated vehicles and reaction time. Phys. Stat. Mech. Appl. 561, 125218 https://doi.org/10.1016/j.physa.2020.125218.

Yang, L., Liu, J., Liu, Z., Luo, W., 2023. Grounding risk quantification in channel using the empirical ship domain. Ocean Eng. 286, 115672 https://doi.org/10.1016/j.oceaneng.2023.115672.

Ye, L., Yamamoto, T., 2018. Modeling connected and autonomous vehicles in heterogeneous traffic flow. Phys. Stat. Mech. Appl. 490, 269–277. https://doi.org/10.1016/j.physa.2017.08.015.

Zhang, D., Lee, K., Lee, I., 2018. Hierarchical trajectory clustering for spatio-temporal periodic pattern mining. Expert Syst. Appl. 92, 1–11. https://doi.org/10.1016/j.eswa.2017.09.040.

Zhang, J., Qian, Y., Zeng, J., Wei, X., Li, H., 2023. Hybrid characteristics of heterogeneous traffic flow mixed with electric vehicles considering the amplitude of acceleration and deceleration. Phys. Stat. Mech. Appl. 614, 128556 https://doi.org/10.1016/j.physa.2023.128556.

Zheng, F., Liu, C., Liu, X., Jabari, S.E., Lu, L., 2020. Analyzing the impact of automated vehicles on uncertainty and stability of the mixed traffic flow. Transport. Res. C Emerg. Technol. 112, 203–219. https://doi.org/10.1016/j.trc.2020.01.017.